



# Detailed map, displacement, paleoseismology, and segmentation of the Enriquillo-Plantain Garden Fault in Haiti

Newdeskarl Saint Fleur\*, Yann Klinger, Nathalie Feuillet

Université de Paris, Institut de Physique du Globe de Paris, CNRS, Paris, France.



## ARTICLE INFO

### Keywords:

Fault mapping  
Offset  
Paleoseismology  
Segmentation  
Enriquillo-Plantain Garden Fault  
Haiti

## ABSTRACT

The Enriquillo-Plantain Garden Fault (EPGF) ruptured several times in Haiti, producing large historical earthquakes (e.g., 18 October 1751, 21 November 1751, and 3 June 1770). Their location and lateral extents are poorly known. The most devastating one, the Mw7.0, 12 January 2010 earthquake should have been the occasion to constrain the fault kinematics and geometry, unfortunately no significant surface rupture was observed. Here, combining LiDAR data, high-resolution aerial photographs, geological map and observations in the field, we revisited the fault map at a large variety of scales to improve the assessment of seismic hazard associated with the EPGF. This detailed mapping allowed us to target several sites for paleoseismic trenches. We carried out paleoseismic investigations in the Clonard pull-apart basin during which one trench was opened perpendicular to the fault. That trench showed stratigraphic evidence for one paleoearthquake. Radiocarbon dating in a dry and buried stream led to the conclusion that the paleoearthquake might be that of 1770. Then, based on kilometric-scale geometric complexities, we showed that the EPGF was composed of more than four segments, each capable to generate  $M_w > 7$  earthquakes. Finally, we identified several geologic and geomorphic markers of long-term deformation along the fault. We found offsets of  $\sim 40$ ,  $\sim 15$  and  $\sim 8$  km from west to east corresponding to slip rates of  $9 \pm 3$ , 4–6 and  $\sim 3$  mm/yr over the Early-Middle Pliocene, Plio-Pleistocene and Pleistocene, respectively. Such a pattern supports the idea of an eastward propagation of the EPGF.

## 1. Introduction

The left-lateral strike-slip Enriquillo-Plantain Garden Fault (EPGF) extends over a length of about 1100 km, with a mean direction of N85°E, from the Cayman Trough to the west, to probably the Enriquillo Valley (Dominican Republic) to the east. It is part of a complex transpressive plate boundary between the North American and Caribbean plates that converge at a rate of about 2 cm/year in a NE-SW direction. This main fault runs on the southern peninsula of Haiti where it is broadly well expressed (Fig. 1) and thus has long been identified [e.g., Duplan, 1975; Mann, 1983; Vila et al., 1985]. Mann et al. (1995) proposed a summary map of the fault, using mainly SEASAT radar imagery and aerial photographs (scale: 1/40000). That map pointed out the main typical geomorphic markers of a strike-slip fault zone such as linear valleys, pull-apart basins and pressure ridges. The fault affects Quaternary deposits, attesting to its activity [Mann et al., 1995]. Several historical earthquakes, in 1701, 1751 and 1770 were attributed to the EPGF, using macroseismic data [Ali et al., 2008; Bakun et al., 2012; McCann, 2006]. Comparing the intensity of the 2010 earthquake to those of the historical ones, Bakun et al. (2012) assigned a  $M_l$  6.6 to the

9 November 1701 event. In 1751 two large earthquakes occurred in southern Hispaniola within one month interval. The first one on 18 October of  $M_l$  7.4–7.5 to the east of the EPGF system may be due to an offshore rupture of the Muertos Trench (Fig. 1, inset). The second one on 21 November of  $M_l$  6.6 occurred near Port-au-Prince is, with less ambiguity, attributed to the EPGF [Bakun et al., 2012]. The 3 June 1770 event, of  $M_l$  7.5, is located broadly to the west of the Lake Miragoâne [Bakun et al., 2012].

Based on the date of occurrence of the last event on the fault and the strain rate indicated by the GPS data, Manaker et al. (2008) estimated that the slip deficit along the EPGF fault was large enough in 2005 that it could break in a near future to produce a M7 class earthquake. Although this was probably verified few years later when the 2010 earthquake occurred (by considering that the rupture broke the EPGF, as inferred by Saint Fleur et al. (2015)), this study was preliminary because 1) the segmentation of the fault had not been considered; 2) the lateral extents of the historical events were not known; and 3) the GPS data did not have enough resolution that would permit to estimate slip rate deficits on separated sections of the fault. To better characterize the seismic hazard associated with the EPGF, paleoseismic studies were

\* Corresponding author.

E-mail address: [newdeskarl@gmail.com](mailto:newdeskarl@gmail.com) (N. Saint Fleur).

<https://doi.org/10.1016/j.tecto.2020.228368>

Received 24 August 2019; Received in revised form 31 January 2020; Accepted 4 February 2020

Available online 06 February 2020

0040-1951/ © 2020 Elsevier B.V. All rights reserved.

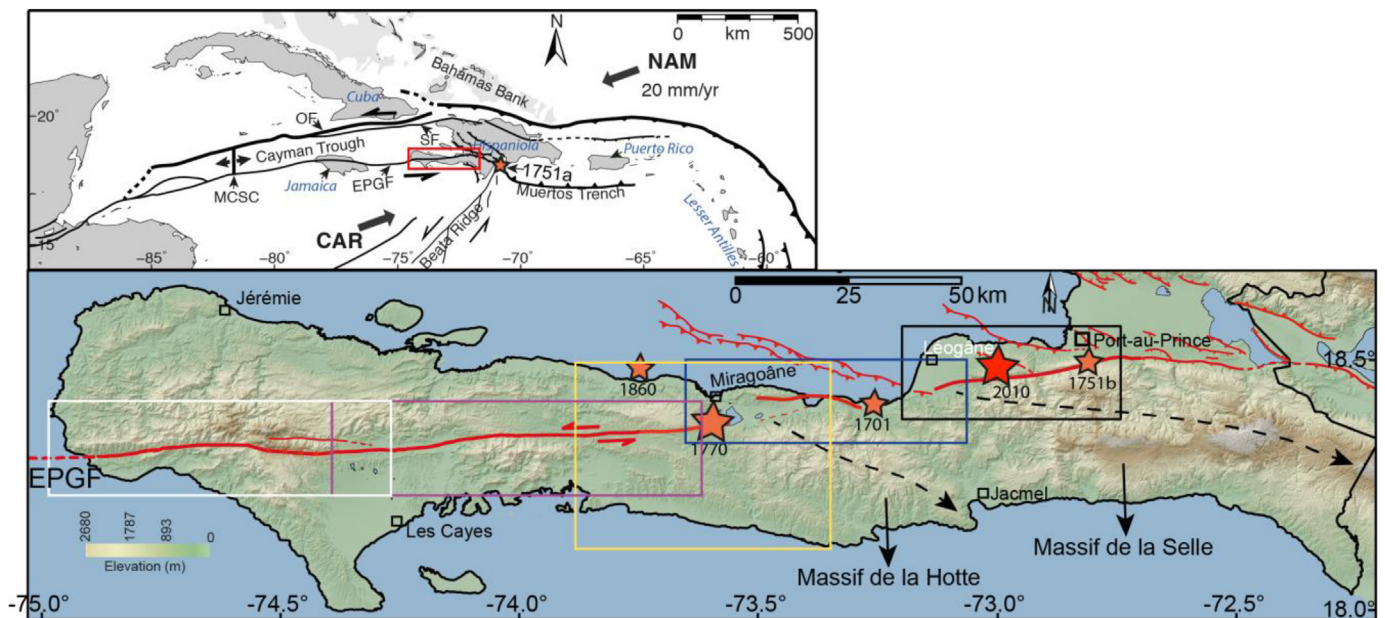


Fig. 1. The Enriquillo-Plantain Garden Fault (EPGF) in southern Haiti. The black, blue, yellow, purple and white boxes are locations of Figs. 2, 7, 8, 10 and 12, respectively. The inset is the tectonic setting of the Caribbean. NAM: North American Plate; CAR: Caribbean Plate; MCSC: Mid-Cayman Spreading Center; OF: Oriente Fault; SF: Septentrional Fault. (For interpretation of the references to colour in this figure legend, the reader is referred to the web version of this article.)

needed. Gold et al. (2012) carried out paleoseismic investigations along the eastern part of the fault, especially, in the Momance Valley and eastern Pétion-Ville (Fig. 2a). The choice of this part of the fault was only based on its geomorphic expression in this area. They excavated three trenches in which they identified recent ground ruptures that might be associated with the 1751 event. Unfortunately, the radiocarbon and luminescence samples yielded ages that could not be interpreted with confidence (Prentice, pers. com., 2013).

In this paper, we mapped in detail the Enriquillo-Plantain Garden Fault, mainly by using high-resolution aerial photographs (pixel 30 cm) and Light Detection and Ranging (LiDAR) data (pixel 1 m) [Van Aardt et al., 2011] complemented with field observations. We first worked at the scale of the southern-peninsula to map the main traces of the fault by using an ASTER Digital Elevation Model (DEM) with a horizontal resolution of 30 m. On the basis of this first-order mapping, we then divided the southern peninsula into five parts to map the fault in much more detail from east to west (Fig. 1). For each part, we gradually decreased the scale of the observations to reach a resolution of few tens of meters depending on the dataset and we combined them to observation in the field when possible. Then, based on criteria of morphological analysis, fault geometry, sedimentary record, and accessibility [e.g., McCalpin, 1996], we selected one site for a paleoseismic investigation. An exploratory trench was excavated and has shown stratigraphic evidence for one paleoearthquake. Indirect radiocarbon dating suggests that this paleoearthquake likely corresponds to an event during the historical period. In addition, we collected information for several other favorable sites for future paleoseismic investigations. Our mapping at all scale eventually allows us for discussing the geometry of the fault and for proposing a first-order segmentation model. The seismic hazard associated with the segments and the geological and morphological offsets along them are also discussed.

## 2. Tectonic background

The formation of the island of Hispaniola is marked by plutonism, volcanism and island-arc metamorphism during the pre-Aptian time. The island-arc (the northern and central parts) has undergone several deformation phases, mainly folding, which was active until the Lower Miocene [Mann et al., 1991a]. A major episode in the formation of

Hispaniola was the suture, in the Lower Miocene, of the island-arc with the southern peninsula [Mann et al., 1991a]. Besides this major episode occurred in Lower Miocene, the sharp escarpments bordering the structures of the island-arc made Mann et al. (1991a, 1991b) suggest transpressive tectonics from the Late Miocene to the present. As the island-arc, NW-SE Lower Miocene folds (e.g., Massif de la Selle, Massif de la Hotte, Fig. 1) have been documented along the southern peninsula of Haiti [Moplaisir and Boisson, 1988; Mann et al., 1991a; Mann et al., 1995]. During the Middle and Upper Miocene time, sandstone, marls and chalky limestone unconformably deposited on the borders of the later folds.

Using magnetic data, Pindell et al. (1988) suggested that the EPGF initiated at the Middle Eocene, propagating eastward from the Mid-Cayman Spreading Center (Fig. 1, inset). The fault seems to have reached the southern peninsula of Haiti at the Pliocene time, disrupting Late Miocene terranes [Wessels et al., 2019; Calais and Mercier de Lépinay, 1995; Calmus, 1983; Calmus and Vila, 1988; Heubeck and Mann, 1991a, 1991b; Mann et al., 1984; Van Den Berghe, 1983; Van den Bold, 1975]. However, based on stratigraphic and structural analyses, Mann et al. (1991b) suggested an earlier episode of E-W strike-slip deformation in the peninsula from the Eocene to the Lower Miocene. This episode would be followed, since the Miocene, by the present-day transpressional regime. Thus, in the Pliocene time, the EPGF would have reactivated old zones of weakness and crosscut en echelon folds along the southern peninsula of Haiti.

About fault segmentation, Leroy et al. (2015) had identified several segments of the EPGF offshore between Haiti and Jamaica using high-resolution multi-beam echo-sounder and shallow seismic reflection data. The segments crosscut pre-existing structures inherited from former tectonic regime [Leroy et al., 2015]. Cowgill et al. (2012) summarized two main segments along the southern peninsula: an eastern and a western segments separated by a huge step-over extended from Fayette to Grand-Goâve bay. They proposed a conceptual model of earthquake behavior along the EPGF. According to that model the 1751b earthquake would have broken the eastern segment from Dumay to Fayette, and the 1770 event would have broken the western segment from Grand-Goâve bay to Clonard pull-apart [Cowgill et al., 2012; Bakun et al., 2012]. The 2010 earthquake would have broken the step-over from Fayette to Grand-Goâve bay, between those two major

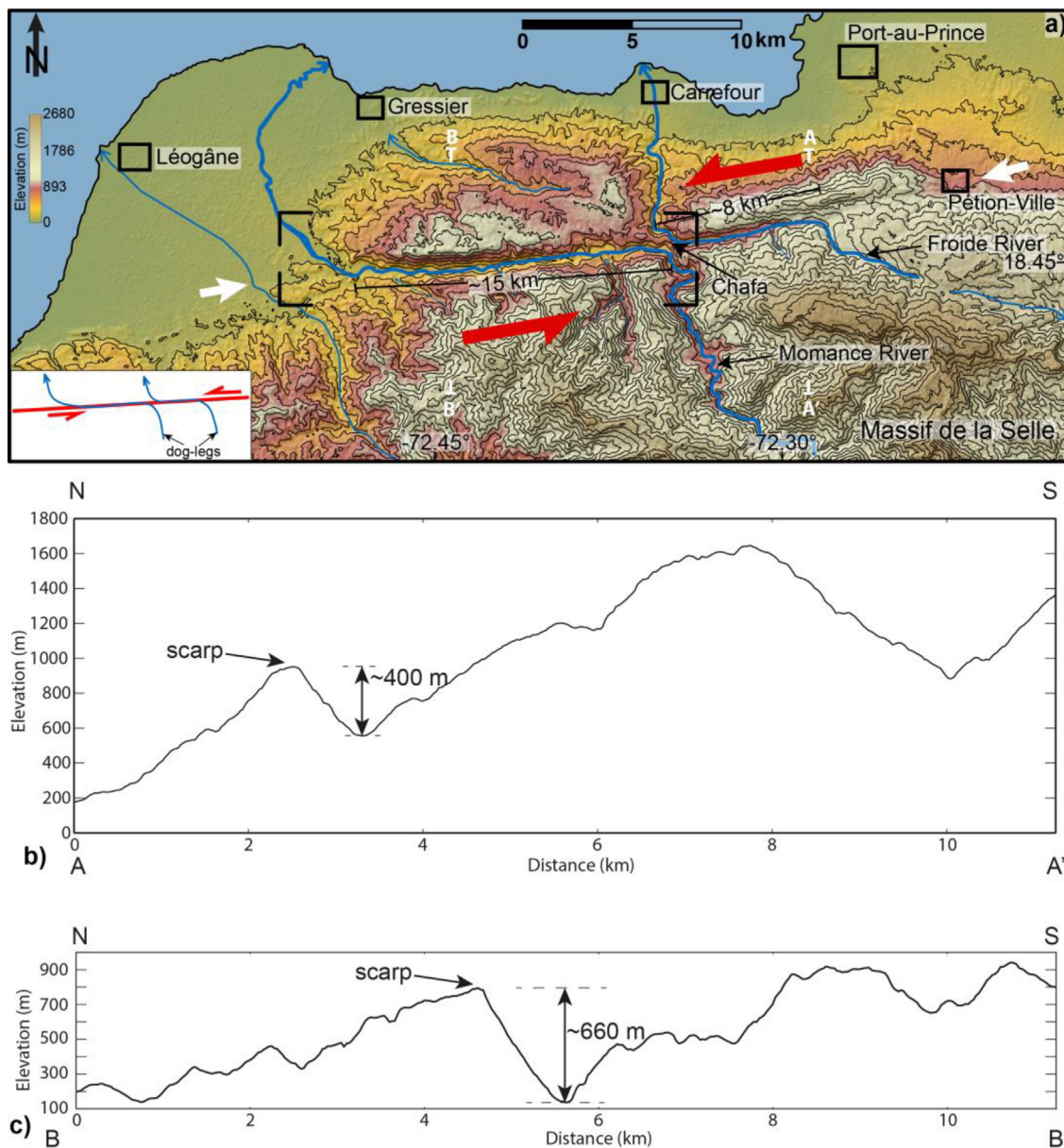


**Fig. 2.** The Enriquillo-Plantain Garden Fault from Léogâne area to Pétion-Ville. In this section, it deflects left-laterally two major rivers, Momance and Froide forming two linear valleys (a). Inset evidences the dog-legs formed by the offset of the rivers. Topographic data: ASTER (pixel: 30 m). Contours are 100-m-interval. b) Topographic profile across Froide river showing an uphill-facing scarp of ~400 m high exhibited by the EPGF. c) Topographic profile across Momance river showing an uphill-facing scarp of ~660 m high exhibited by the EPGF.

segments [Cowgill et al., 2012]. After the 2010 Haiti earthquake, several studies have focused on the area of Léogâne and the Cul-de-Sac plain. Using high-resolution topographic data and aerial photograph Saint Fleur et al. (2015) mapped in detail faults around the epicentral area of the 2010 earthquake. We found that the strike-slip deformation induced by the EPGF stops near Pétion-Ville, southern Port-au-Prince and then a WNW-ESE fold and thrust network prevails eastward. That pattern was confirmed by Calais et al. (2016) using GPS data. They highlighted a strong component of shortening around the Cul-de-Sac basin, while the GPS vectors are nearly parallel to the EPGF fault trace western Léogâne. Saint Fleur et al. (2019) analyzed the drainage network and found that the paleofan of Port-au-Prince was offset by ~8 km across the EPGF. In addition to the strike-slip deformation, we used high-resolution topographic data, aerial photographs, geological information and field observations to map in detail the WNW-ESE folds and thrusts in Port-au-Prince and the Cul-de-Sac – Enriquillo plain. A model of nearly pure strike-like from Tiburon to Pétion-Ville, then

transpression and compression on the Dumay Fault and on the Bahoruco Fault, respectively, was inferred [Saint Fleur et al., 2019]. Seismicity, focal mechanism and crustal structure analysis in southern Haiti revealed a transition in the EPGF system from a near vertical strike-slip fault along the southern peninsula to a southward-dipping oblique-slip fault along the southern border of the Cul-de-Sac-Enriquillo basin (Possee et al., 2019; Rodriguez et al., 2018). In the lake Azuéi Cormier et al. (2019) acquired 220 km of multichannel seismic reflection profiles across its surface. They found two major structures: a NW-SE fold bounds the western side of the lake and another one to the southern side. The latter is poorly imaged below a shallow gas front [Cormier et al., 2019]. However, the study of Wang et al. (2018) proposed that the folds are produced by shear along the EPGF that would continue all along the Cul-de-Sac – Enriquillo basin including in the lake Azuéi.

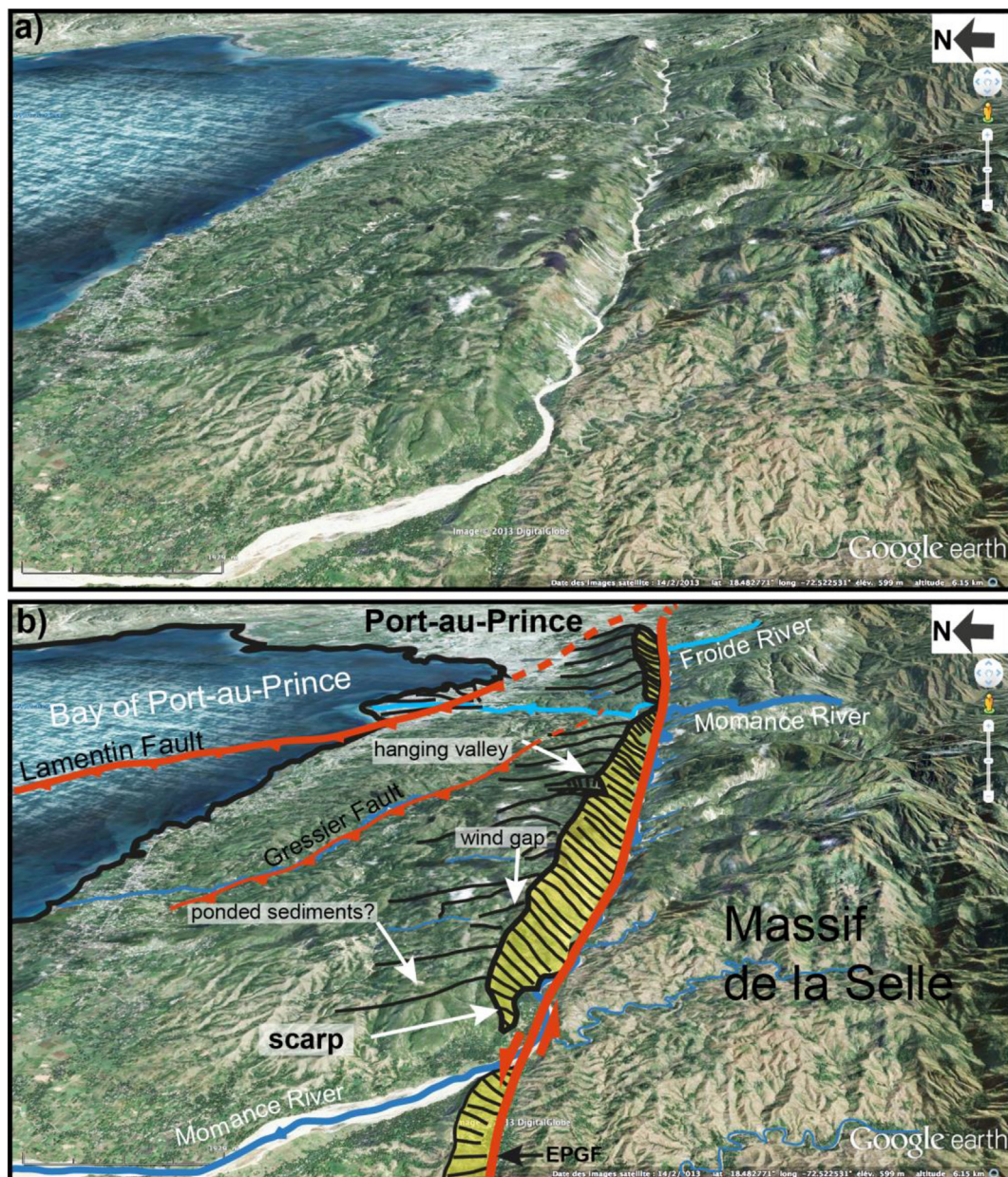


**Fig. 3.** Eastward view of the EPGF scarp. a) Google Earth 3D eastward view of the Momance river and the Froide river Valleys and interpretation. The Enriquillo-Plantain Garden Fault and the Lamentin thrust bound an uplifting block which is limited to the south by a ~35 km long, up to 700 m high, linear and steep uphill-facing scarp (in yellow in b). The scarp acts as a shutter ridge blocking the drainage and diverting the main rivers (Momance and Froide, in blue). (For interpretation of the references to colour in this figure legend, the reader is referred to the web version of this article.)

### 3. Detailed mapping of the EPGF

#### 3.1. The Momance Valley

The Froide and Momance rivers are the most prominent drainages controlled by the EPGF in the southern peninsula. The valleys of the latter rivers are linear and mark the morphology (Figs. 2–5) [Mann et al., 1995]. Fig. 2a shows that the fault is morphologically well expressed along the Pétion-Ville - Léogâne section where the main rivers (Momance and Froide) are left-laterally offset by the fault to form two dog-legs (Fig. 2a, inset). In the area where the valleys are running parallel to the fault, the latter is ~35 km long, up to 700 m high, linear, and has a steep uphill-facing (i.e. south-facing) scarp (Figs. 2, and 3). The scarp portrays numerous geomorphic features of ongoing uplift north of the EPGF surface trace. The sharp uphill-facing EPGF scarp is incised by numerous small, narrow, intermittent gullies, some flowing

in perched wineglass valleys, implying that transverse stream incision has not kept pace with relative tectonic uplift (Fig. 4) [Saint Fleur et al., 2015]. In addition, numerous wind gaps, ponded sediments, upstream of deep gorges incised by streams flowing toward the bay of Port-au-Prince may indicate a drainage reversal due to tectonic uplift. Overall, the Enriquillo-Plantain Garden Fault and the Lamentin thrust bound an uplifting block which is limited to the south by the salient EPGF scarp [Saint Fleur et al., 2015].

The two drainages (Momance and Froide) are separated by a 500-m-wide, elongate ridge (Chafa). West of the Chafa ridge, on two meanders of Momance river, we can observe a sharp uphill-facing scarp through the limestone (Fig. 5b, c, Fig. S1a, b) mapped as Eocene [Bien-Aimé Momplaisir, 1986].

On the eastern meander and on the southern wall of Momance river, a ~N75°E fault has been identified [Lacassin et al., 2013; Prentice et al., 2010]. This fault exhibits a ~5-m high uphill-facing scarp evidenced by

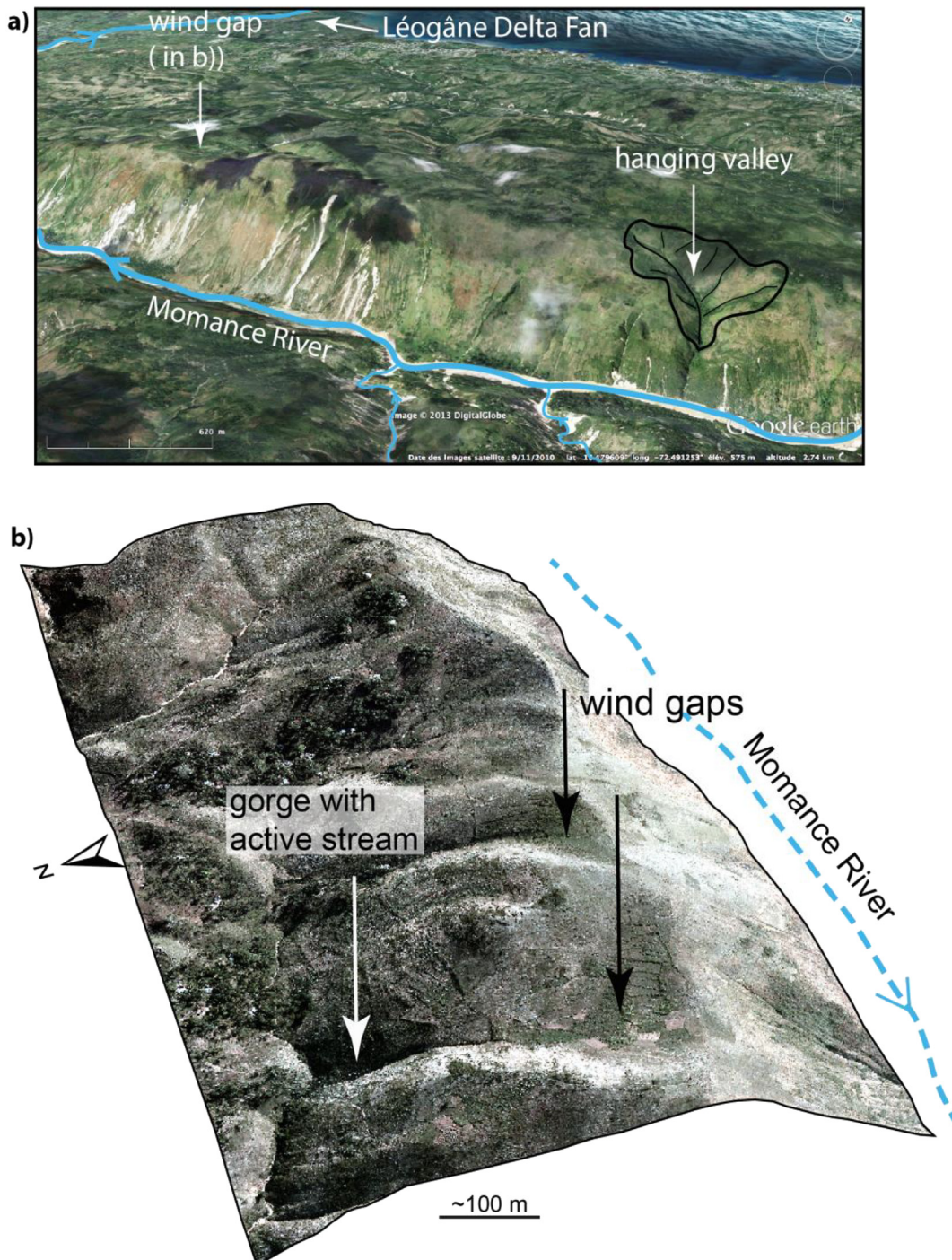


**Fig. 4.** Geomorphic markers of on-going uplift north of the EPGF. a) The sharp uphill-facing Enriquillo-Plantain Garden Fault scarp is incised by numerous small, narrow, intermittent gullies, some flowing in perched wineglass valleys, implying that transverse stream incision has not kept pace with relative tectonic uplift. b) Northeastward view on a part of the crustal block uplifted between the EPGF and the Lamentin Fault. The image was elaborated using aerial photograph (with a spatial resolution of 30 cm) superimposed on ASTER topography (spatial resolution: 30 m) with no vertical exaggeration.

an orthogonal topographic profile on the LiDAR DEM (Fig. 5b, inset). The fault blocks and deflects the tributaries of the main river. In the center-east of Fig. 5b, we note the clearest offset tributary that exhibits a nice dog-leg. As we consider that the stream has been offset because of slips on the fault during several earthquakes, we tentatively reconstruct, by back-slipping, its initial geometry. Since we mapped the boundaries of the terraces of the stream, they can be used as piercing lines. The terraces are the abandoned beds of the stream. Thus, we can infer that the stream used to flow along those terraces before being offset. We first consider that the stream used to flow along the western

terrace of the downstream; we match the upstream to the border of this western terrace. We obtain a maximum offset of about 60 m (Fig. S1c). A minimum offset of about 48 m is also obtained by matching the upstream to the border of the eastern terrace (Fig. S1d). But, the most probable reconstruction is done by corresponding directly the upstream to the downstream. This reconstruction yields an offset of about 55 m (Fig. 5b, Fig. S1e). This reconstruction appears to put the western and the eastern terraces of the downstream in front of those of the upstream. Our most probable offset measurement is comparable to the 52 + 18/ - 13 m of Cowgill et al. (2012), using LiDAR data. In this area, minor

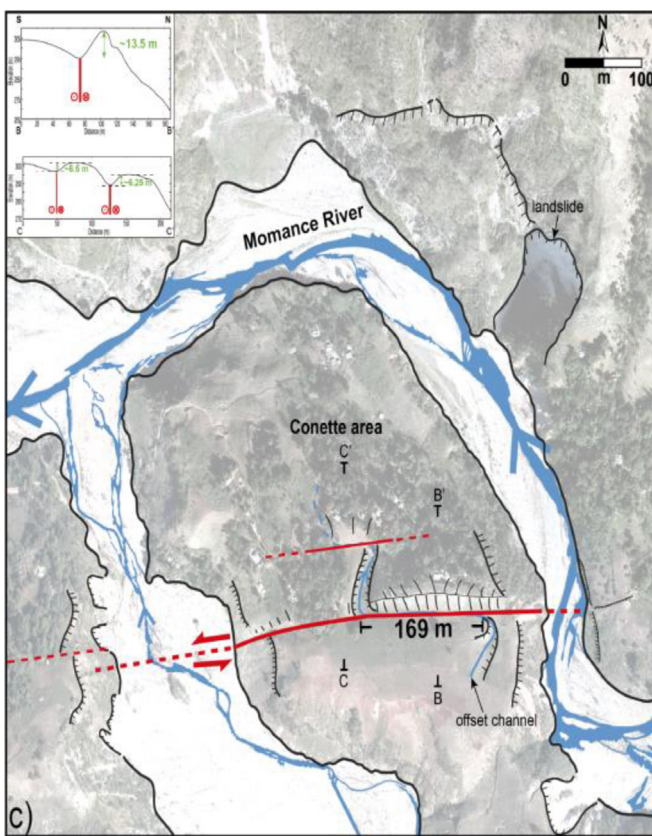
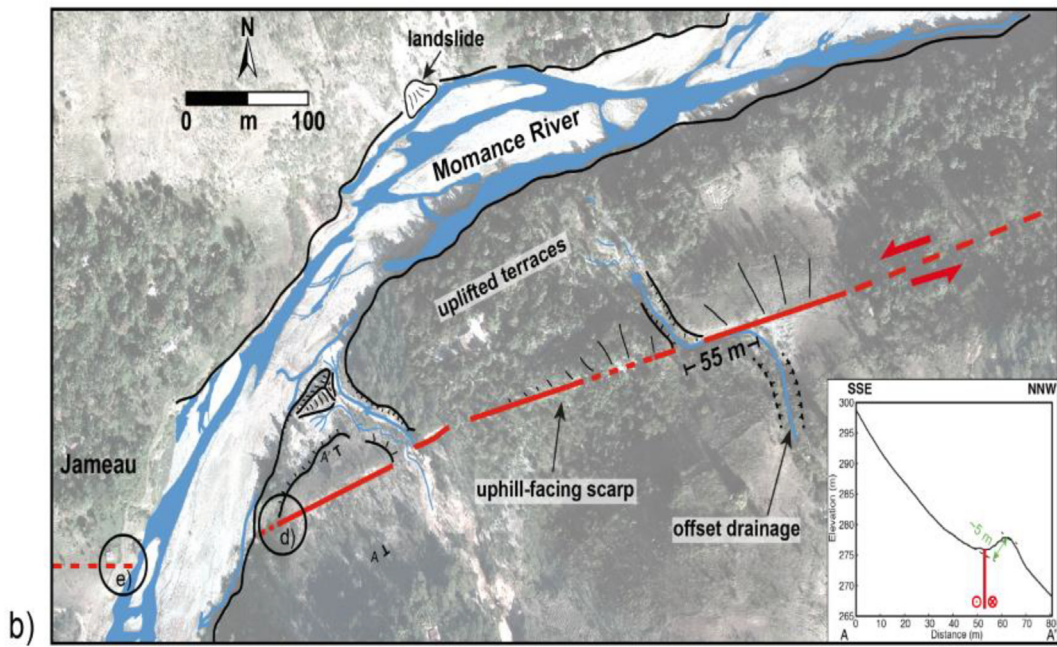
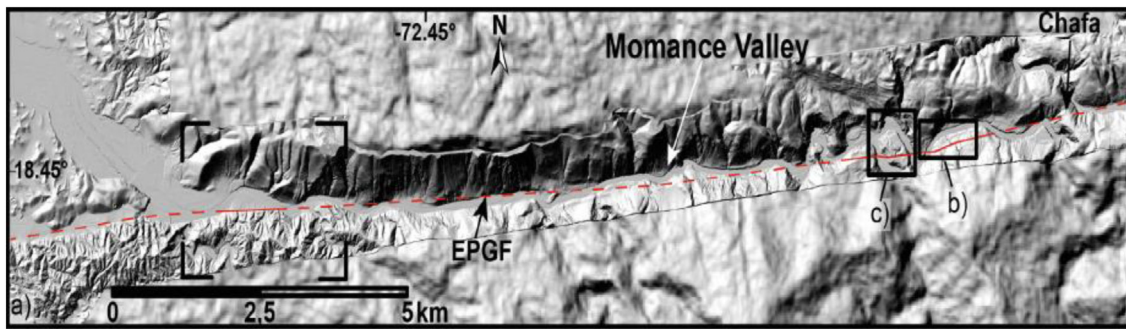


**Fig. 5.** a) The linear Momance Valley controlled by the Enriquillo-Plantain Garden Fault (EPGF). LiDAR data (pixel: 1 m) overlain on ASTER data (pixel: 30 m). The westernmost black box locates Fig. 6. b) Aerial photograph (pixel: 30 cm) and interpretation of fault-related features on a meander to east of Jameau area. The fault exhibits uplifted alluvial terraces and offset drainages. Inset shows a topographic profile along the uphill- south-facing scarp of the fault that is about 5-m high. The topographic profile was extracted from the LiDAR DEM. c) Aerial photograph and interpretation of the Conette area, western Jameau. This area shows an offset dry channel (in foreground). The same channel seems to be offset again by a minor fault (in background). d) Fault exposure in eastern Jameau area. The geometry ( $\sim$ N100°E, 60°S) of this fault presents a drastic change, compared to that in e) located at < 100 m (see text for discussion). e) Field photograph of the western edge of the eastern meander showing the uphill- south-facing scarp suggesting a north dip of the fault in this area.

lateral offsets (1.8–2 m) have also been measured in the field [Prentice et al., 2010] and may be associated with one historical earthquake. This morphology is well preserved in spite of the high erosion rate in the region. At that scale the geometry of the fault is quite ambiguous. Indeed, at the westernmost border of this eastern meander, our field observations confirm an uphill - south-facing scarp (Fig. 5d) suggesting a north-dipping fault, assuming that the fault has a small reverse component in this area. However, in < 100 m to the west, at eastern Jameau, the fault exposes a  $\sim$ N100°E, 60°S plane on the northern wall of Momance river (Fig. 5e) [Prentice et al., 2010; This study].

At the Conette site (the western meander), a N84°E fault is observed. Topographic profile on the LiDAR data shows that the fault scarp is about 13.5-m high (Fig. 5c, inset). This fault clearly offsets left-laterally a channel. We tentatively propose to reconstruct this channel. We first, by back-slipping, put the eastern terrace of the upstream in front of the western terrace of the downstream. We obtain the maximum possible offset of about 203 m (Fig. S2c). This maximum offset may be over-estimated, as it is simpler to match the western terrace of the upstream to the western terrace of the downstream. In the same manner, we propose a minimum possible offset of about 158 m (Fig. S2d). Indeed, this minimum offset is obtained by putting the western terrace of the upstream in front of the eastern terrace of the downstream. It is thus the least offset we can get. More realistically, we try to match the southern part of the downstream and the northern part of the upstream, following their general direction. This reconstruction yields an offset of about 169 m (Fig. S2e). It is our best reconstruction and is compatible with the 163 m found by Prentice et al. (2010) using field measurement. We can follow this channel northward where it abuts against another less significant E-W fault scarp. This scarp is  $\sim$ 6.5-m high (Fig. 5c, inset). The channel appears to be also offset by this second fault.

### 3.1.1. The site of Fayette (Jean-Jean)

The site of Fayette is located at the western outlet of the linear Momance Valley. This site is at the junction of at least three geologic formations (Fig. 6a). At this place, the fault passes through the basement (Cretaceous basalt) of the southern peninsula and continues eastward through the Eocene limestone. North of the fault trace, the village of Fayette is built on a terrace of Momance river. This northern part is less eroded than the southern one. Several landslides, which are probably induced by the 2010 earthquake [Gorum et al., 2013], are observed at the base of the less eroded northern part. On a 3D view of the area of Fayette (Fig. 6b) we can see that mounds on the southern wall of Momance river are clearly truncated by a linear fault. The drainage network that is coming from the southern block undergoes strike-slip deformation. Indeed, detailed mapping of this area shows offset, deflected and beheaded channels (Fig. 6c). Some of the drainages stop abruptly at the piedmont of the mountain, near the fault scarp. They abut against fans, probably their own fans, without re-incising them. Few tens of meters toward the north, we find other incisions with no clear catchments. Such a pattern may indicate that the fans are abandoned. The upstreams, instead of re-incising the fans, would infiltrate at the fault scarp and reappear further north.

In this site of Fayette, Prentice et al. (2010) measured in the field 7 minor channel offsets. They are ranging from 1.3 to 3.3 m. Those offsets may be associated with one of the eighteenth century earthquakes [Prentice et al., 2010].

### 3.2. Léogâne-Miragoâne Complex Zone

From Léogâne to Miragoâne, the Enriquillo-Plantain Garden Fault consists of a  $\sim$ 45-km long zone of geometric complexities (Fig. 7a). The fault is well expressed along the Momance Valley. In contrast, from Fayette to Dufort the fault is not well expressed, except the sharp topographic limit between the basalt of the Massif de la Selle and the Quaternary deposits of Léogâne Delta Fan. From Dufort, no strike-slip deformation is clear over a distance of  $\sim$ 17 km until the town of Grand-Goâve where evidence for reverse faulting is rather seen. To the south of the town of Grand-Goâve, a linear hill front is observed, separating Pliocene rocks to the south and Quaternary deposits to the north (Fig. 7b). On the hill, we identified several hanging valleys that attest to active reverse faulting. Fig. 7c shows details of an old tributary of Grand-Goâve river. This tributary left its ancient trace on the hill characterized by alluvial material in a sinuous depression. This environment is quite favorable for dense low vegetation. Following this vegetation, we reconstituted the trace of the old stream until its paleofan. This valley is perched at  $\sim$ 100 m.

West of Grand-Goâve, the strike-slip fault reappears along the  $\sim$ N110°E Tapion pressure ridge (Fig. 7d). This typical spindle-shaped restraining bend is bending by about  $\sim$ 17° of the fault in this area. The fault may have first formed the pressure ridge and offset it later or simultaneously. As a restraining bend, the Tapion pressure ridge may be bordered by secondary thrusts. Hence, an offshore thrust may explain the abrupt northern coast of Tapion where numerous landslides and uplifted coral reefs were observed (Fig. 7e).

From Tapion pressure ridge, the EPGF likely continues offshore for only about 4 km before being quite visible onland along the southern flank of Fort-Royal hill. At this place, the fault marks the morphology by a linear slope break. Similarly to Tapion pressure ridge, the northern coast of Fort-Royal hill is abrupt and exhibits uplifted beaches (Fig. 7f). The beaches are uplifted by up to  $\sim$ 4 m. These observations may be compatible with an offshore thrust, likely the Trois-Baies Fault, bounding the hill (Fig. 7a).

After running along southern Fort-Royal, the EPGF steps down to form an up-to-5-km wide and 20-km long depression: the Miragoâne pull-apart. With about 43 m depth, the lake Miragoâne, the main feature of the pull-apart, is the deepest lake of the caribbean [Brenner and Binford, 1988; Higuera-Gundy et al., 1999; Wang et al., 2018]. Sonar survey in the lake revealed that the sediments are highly deformed mainly by normal faulting, typical of a pull-apart basin [Wang et al., 2018]. Core and pollen data from the lake Miragoâne revealed that the formation of the pull-apart would be at least 43kyr [Wang et al., 2018].

### 3.3. Fond-des-Nègres area

West of the Léogâne-Miragoâne Complex Zone (LMCZ), in the middle of the southern peninsula, the EPGF is very well expressed and has a clear single trace in the morphology. A hillshade image of an ASTER DEM superimposed by the 1/250000 geologic map of Haiti [Momplaisir and Boisson, 1988] enables us to combine the information given both by the topography and the geology (Fig. 8). The fault cuts across the southern flank of Rochelois plateau and juxtaposes the Cretaceous and Paleogene units composing the plateau and Neogene units and Quaternary deposits which found in Fond-des-Nègres basin. North of the town of Fond-des-Nègres, the fault exhibits a  $\sim$ 24-m-high uphill-

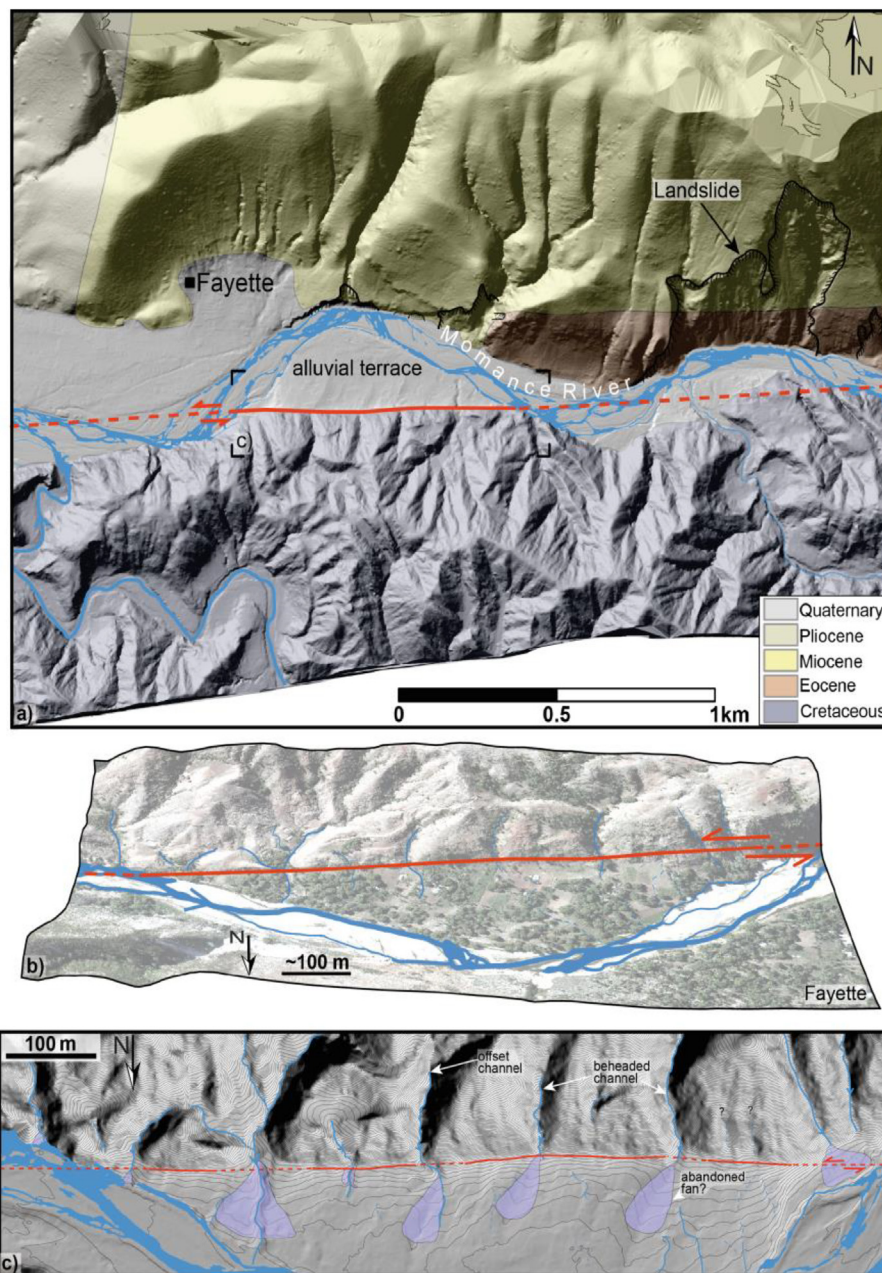


**Fig. 6.** a) Geomorphic map of Fayette area. The geologic map (scale: 1/250000) [Momplaisir and Boisson, 1988] is overlain on LiDAR DEM (pixel: 1 m). The black box is the location of c). b) 3D view of Fayette (Jean-Jean) area, looking to the south. In this area, the fault is well expressed in the morphology. The image is made of aerial photograph (pixel: 30 cm) overlain on LiDAR DEM (pixel: 1 m). c) Topographic map showing the disturbance (e.g., offset channel) created by the EPGF in Fayette area.

facing (i.e. north-facing) scarp (section AA', Fig. 8b, inset). The fault continues westwards where it offsets a part of the drainage network: many small gullies that flow southward, on the northern compartment of the fault, are disrupted by the fault and remain confined on its northern side instead of flowing into the main Serpente river (Fig. 8b). We observe the same feature eastward in the Jacquot area as highlighted by very high-resolution aerial photograph (pixel 30 cm, Fig. 9). At this scale, the fault trace is long and linear and made of several few kilometer-long small segments. We can observe that the drainage network flowing from the Rochelois plateau is also disrupted by the fault. As a result, several ponds and small basins have developed along the fault scarp. East of this area, we can observe that some gullies are even deflected in a sinistral sense before flowing into the ponds. The Fond-des-Nègres area, especially the three basins shown in Fig. 9a, has been

investigated in the field for further paleoseismological studies. In the following we described in more detail one of these sites (Ka' Jacquot pond, Fig. 9b).

### 3.3.1. Ka' Jacquot pond area

In the Ka' Jacquot pond area, the EPGF cuts across Paleogene limestones, highly eroded due to intense tropical rainfalls. Its scarp is high enough (> 10 m high) to block the drainage network, forcing the water to flow along its base before filling one of the small basins. The southward view of the landscape (Fig. 9b) strikingly illustrates this relationship. We can clearly distinguish a well-developed alluvial fan of a stream that abuts against the scarp. We inferred that the stream used to flow downward toward the lower topographic points (beyond the scarp to the south) before having been blocked by the progressive

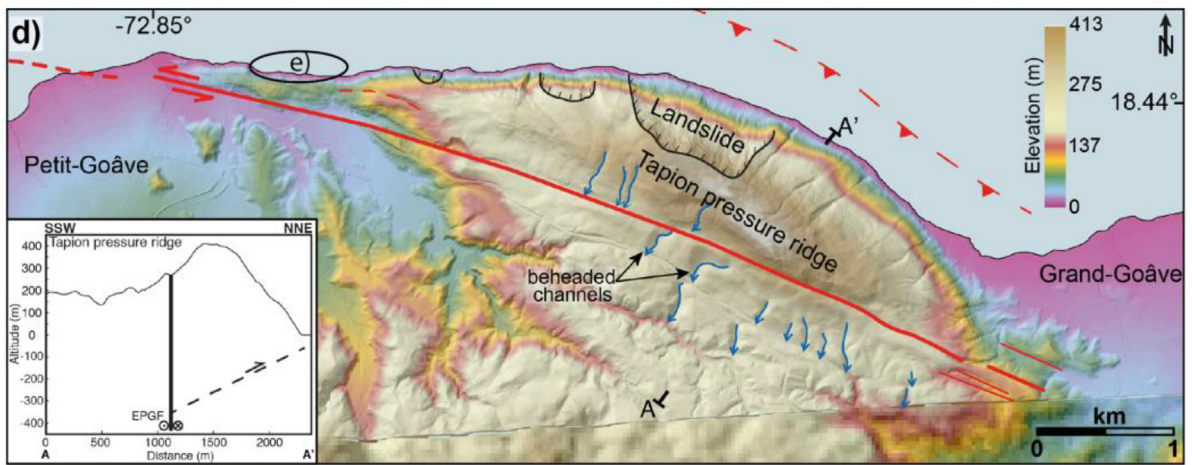
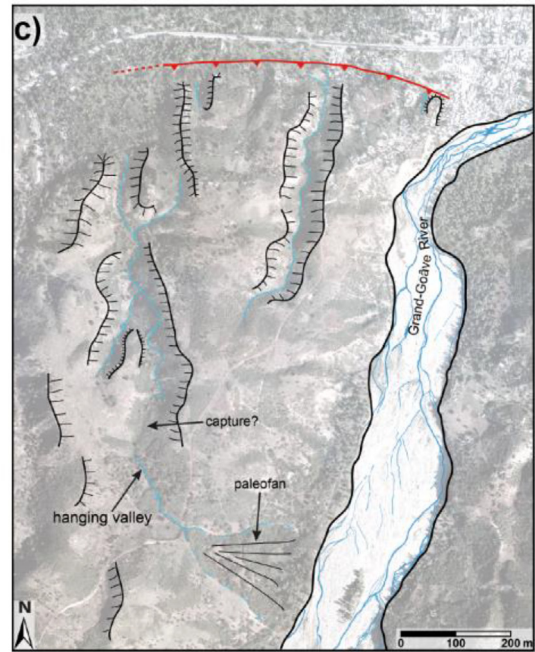
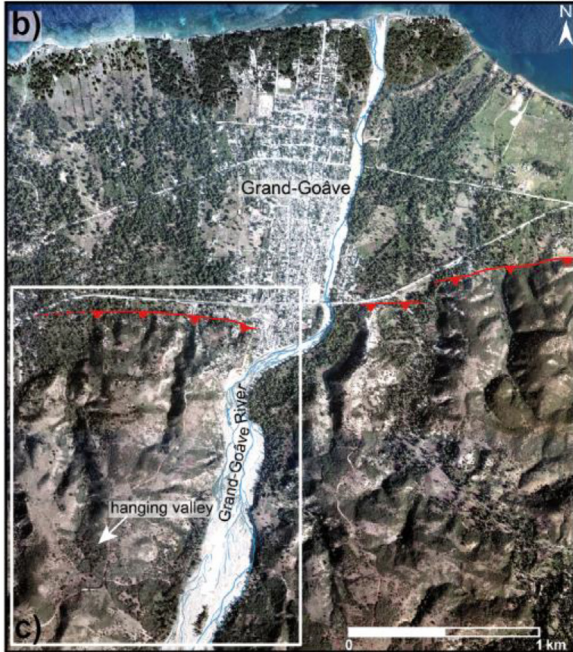
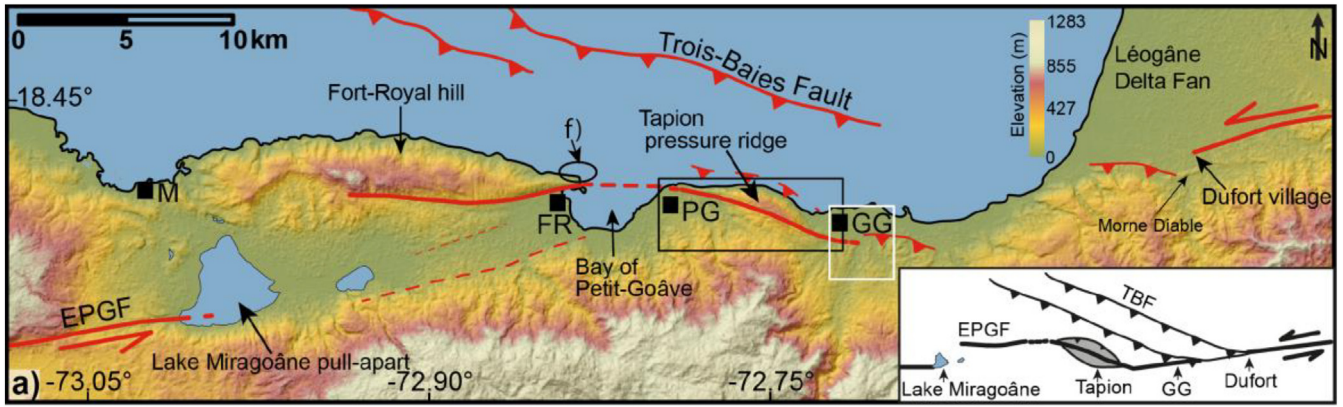


**Fig. 7.** a) The Léogâne-Miragoâne Complex Zone. It is marked by a ~45 km long geometric complexities, including the Lake Miragoâne pull-apart, the Tapion pressure ridge and the Grand-Goâve - Dufort zone of diffuse deformation. White and black boxes are locations of b) and d), respectively. Inset is our interpretation of the possible connection of the Trois-Baies Fault (TBF) system to the Enriquillo-Plantain Garden Fault (EPGF). FR: Fort-Royal; PG: Petit-Goâve; GG: Grand-Goâve. b) Grand-Goâve area where the EPGF is not clear and rather replaced by compressive deformation. The white box is the location of c). c) shows evidence of geomorphic features (e.g., hanging valley) that suggest vertical motion in this area. Data: aerial photograph (pixel: 30 cm). d) The spindle-shaped Tapion pressure ridge (> 400 m high). It is formed by a right step bend of ~17° of the EPGF. The landslides occurred prior to and during the 2010 Haiti earthquake. Inset is our proposed geometric relationship between an inferred offshore thrust and the EPGF. The surface emergence of the inferred offshore thrust is out of the frame of the cross-section. Data: LiDAR DEM (pixel: 1 m). e) Field photograph showing uplifted coral reefs along the northern coast of Tapion. f) Uplifted beach exposed on the northern coast of the hill of Fort-Royal. This beach is about 4-m high.

growth (by cumulative slips) of the EPGF fault scarp. This scarp now acts as a shutter ridge forcing the water to flow more eastward into the Etang Ka' Jacquot basin. This process is confirmed by the extent of the alluvial fan eastward. The intensive erosion by the water flow contributes to increase the height of the scarp enhancing the effect of the tectonics. West of the alluvial fan the fault scarp gradually decreases in height (Fig. 9a). In any case, the fault is active enough to defeat the whole drainage network in this area.

### 3.4. L'Asile, Clonard pull-apart and Camp-Perrin basins

L'Asile basin is located between the Rochelois plateau to the east and the Clonard basin to the west (Fig. 10a). It is filled with continental Miocene units which lie unconformably upon the older Cretaceous folded units [Bien-Aimé Momplaisir, 1986]. In this area, the scarp of the EPGF is less clear than in other sites. However, it can be evidenced by analyzing slight variations of slopes in the basin (Fig. 10b). The basin can be clearly distinguished in the slope map because it forms a rather flat area (with slopes ranging between 0 and 36%) compared to the surrounding higher reliefs. It is crosscut by discontinuous few kilometer-long linear E-W-striking slope breaks (between 0 and 18%), which highlight the fault trace. West of the basin, a linear E-W-striking slope break is continuous over 5 km. It corresponds in part to the Citronnier riverbed which course is deflected and controlled by faulting (Fig. 10c). Along this 5 km long portion, the direction of the fault veers progressively by 4° clockwise before cutting in the middle of Clonard basin westward. (Fig. 10c).

We infer that this basin is a ~24-km<sup>2</sup> spindle-shaped pull-apart along the EPGF. In the middle of the Clonard basin the main fault is well-expressed and exhibits a well-preserved ~2-m high scarp in the Quaternary alluvium (Fig. 13). In this area, the fault controls the course of the main river (Cavaillon) flowing from the basin of Camp-Perrin (Fig. 11a). The Camp-Perrin and Clonard basins are connected by the wide Cavaillon river bed, overall forming a ~30-km long and up-to-5-km wide depression. This depression is filled with Quaternary sediments brought by numerous active rivers (e.g., Bonne Fin, Gros Marin) which all converge toward this area. The basin of Clonard, in particular, is completely filled with Late Quaternary sediment which are offset by faulting attesting for Late Quaternary faulting. West of the Clonard basin, several meanders and terraces of Cavaillon river are crosscut by the fault. In such areas, the terraces of the rivers are probably flooded regularly but the scarp is still well preserved attesting for recent activity along the fault. Near one of the westernmost meanders of the river on Fig. 11c, a minor pull-apart basin (Laplace) is formed by a 140-m left step-over of the main fault. This little basin is not bounded by two fault sections but it expands widely to the north and slightly to the south of the fault traces. Because the basin consists of a good sediment trap, it is preferentially used for agriculture.

### 3.5. Macaya pressure ridge and Tiburon River

West of Camp-Perrin, the direction of the EPGF veers counter-clockwise by 10° where it bounds the southern flanks of Macaya mountain. The highest point of this mountain is the Macaya peak (2347 m), which is the second highest peak of Haiti (Fig. 12a). Another secondary fault (Ravine du Sud Fault, RSF), is identified to the north of

the main EPGF and controls the course of the Ravine du Sud river [Calmus, 1983; This study]. The latter river flows in an ~E-W direction before abruptly veering to flow southward along the western border of the Camp-Perrin basin. A 20 km-long, 3 km wide, ~2.2-km high, ~N95°E elongate ridge is caught in between the RSF to the north and the main EPGF to the south. Although, as most of the Macaya mountain, this relief is partly inherited from earlier Laramide folding [Calmus and Vila, 1988], the faults may have contributed to shape and enhance the relief of the ridge which we inferred to be mainly a pressure ridge of the main EPGF. The shape and direction of the ridge is consistent with the overall geometry of the fault zone.

To the west of the Macaya pressure ridge, the EPGF continues linearly and controls the course of the main rivers (e.g., Tiburon River). Fig. 12b shows an aerial photograph of the area of Nan Cosse River. The fault clearly encroaches the southern terraces of that east-flowing river before stepping down along the west-flowing Tiburon River. From there, the Tiburon River runs along the EPGF, forming a linear valley. Then, the fault continues offshore.

## 4. Paleoseismic investigations – identified potential sites

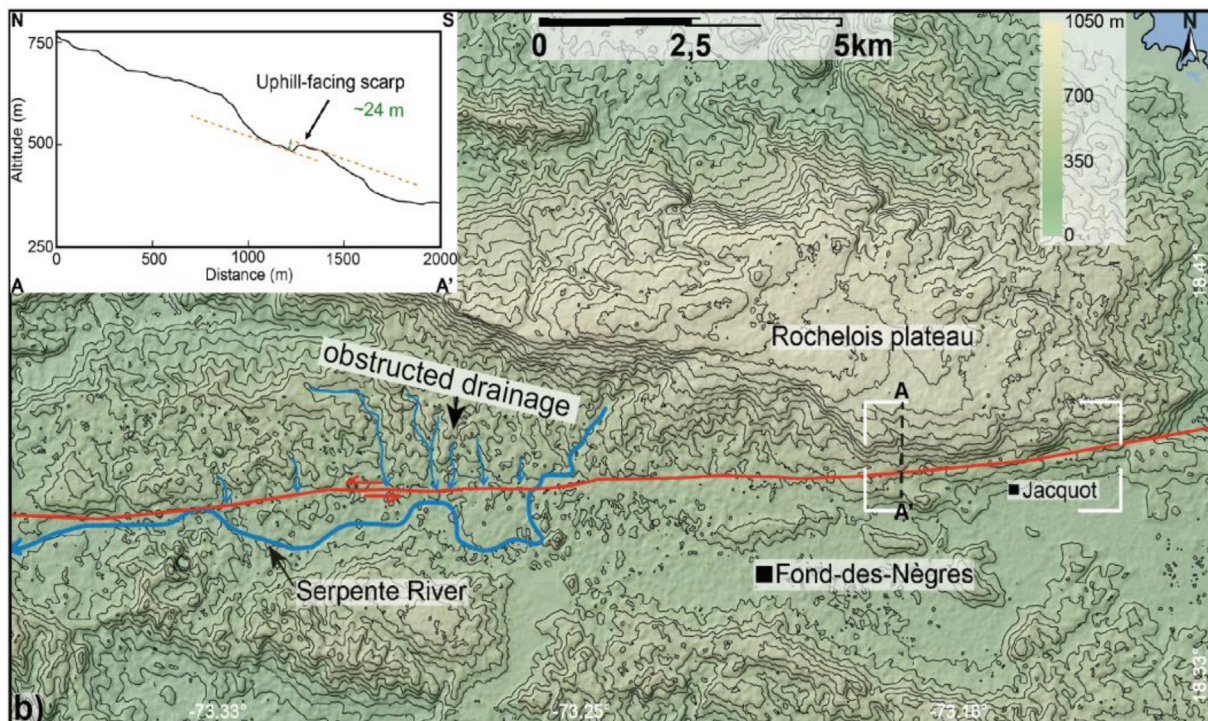
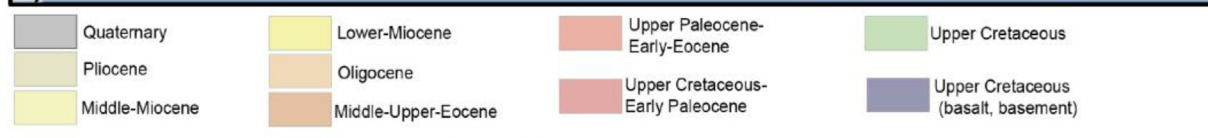
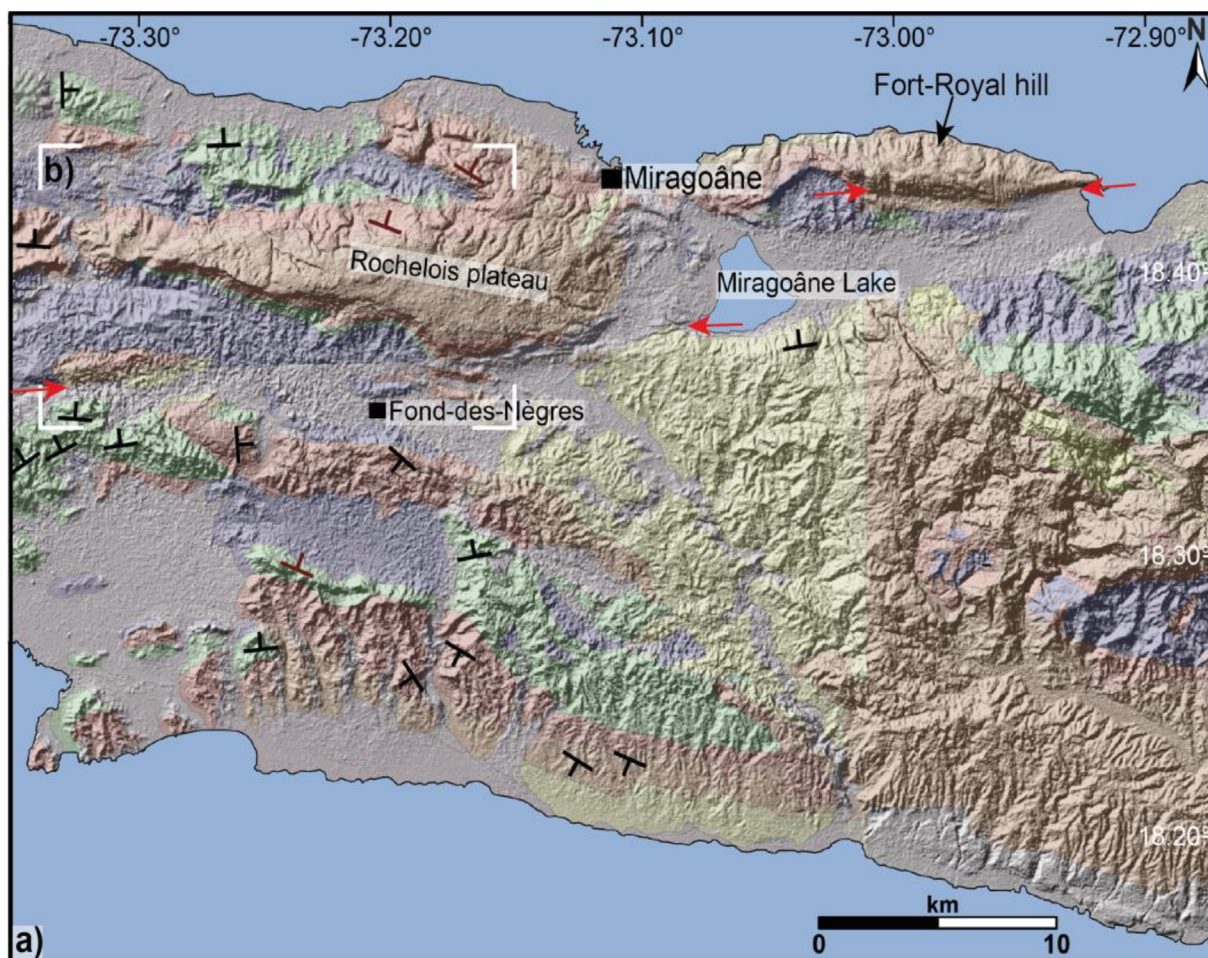
During our fault mapping, we identified several potential sites for paleoseismological studies (Table 1). In the areas of Fond-des-Nègres and L'Asile basin the sites were overall inappropriate because of limestone outcrops along the fault scarp. However, the eastern Jacquot area and the Clonard basin particularly show better stratigraphic criteria for paleoearthquake records because the different soil units are relatively thin and clear (Fig. S3). In particular, the basin of Clonard is likely a closed basin where the sedimentary record should be well preserved. (Fig. 11). In addition, the fault scarp is well expressed in the Quaternary alluvium.

### 4.1. Site selection

At the western edge of the Clonard basin, we identified two favorable sites especially in the area of the Cavaillon River: 1) the Laplace small pull-apart described earlier (Fig. 11c); and 2) The Siline area, where an alluvial terrace is crosscut by the fault, which scarp is ~2-m high at this place (Fig. 13), consistent with the observations made further east by Mann et al. (1995). We selected the Siline site because: 1) the fault has a simple geometry; 2) the area is well fed in sediment; 3) despite unfavorable conditions such as erosion, flooding and agricultural activities, the fault marks the morphology, attesting to Late Quaternary activity; and 4) the site is quite accessible.

### 4.2. Excavating an exploratory trench

As we were satisfied by the morphology and the stratigraphy exposed along riverbeds we could excavate manually an exploratory trench (Fig. 13c). This trench is ~14-m long, 1.5-m wide and 1.5-m depth. Fig. 14 shows the eastern wall of the trench that exhibits fine alluvial materials. The stratigraphic units were not very sharp but we could distinguish at least 5 different units, a sixth one being the arable soil. From the bottom to the top, the first unit is a sandy light greyish unit. This unit is topped by yellowish, blackish, dark greyish, and brownish silts and clays. The uppermost unit is the organic soil made of



(caption on next page)

**Fig. 8.** a) Geologic units crosscut by the EPGF (red arrows) in the middle of this part of the peninsula. White box is the location of (b). The geologic units are redrawn from the original map (scale: 1/250000) [Momplaisir and Boisson, 1988] and overlain on ASTER shaded DEM (pixel: 30 m). The dip directions drawn in black are from the original geologic map, those in brown are inferred using Google Earth imagery. b) Fonds-des-Nègres area. To the west, the drainage network is captured by the fault. Inset is a topographic profile showing a ~24-m uphill-facing scarp. Such morphology makes that the fault blocks the south-flowing drainage network shown in Fig. 9. White box is the location of Fig. 9.

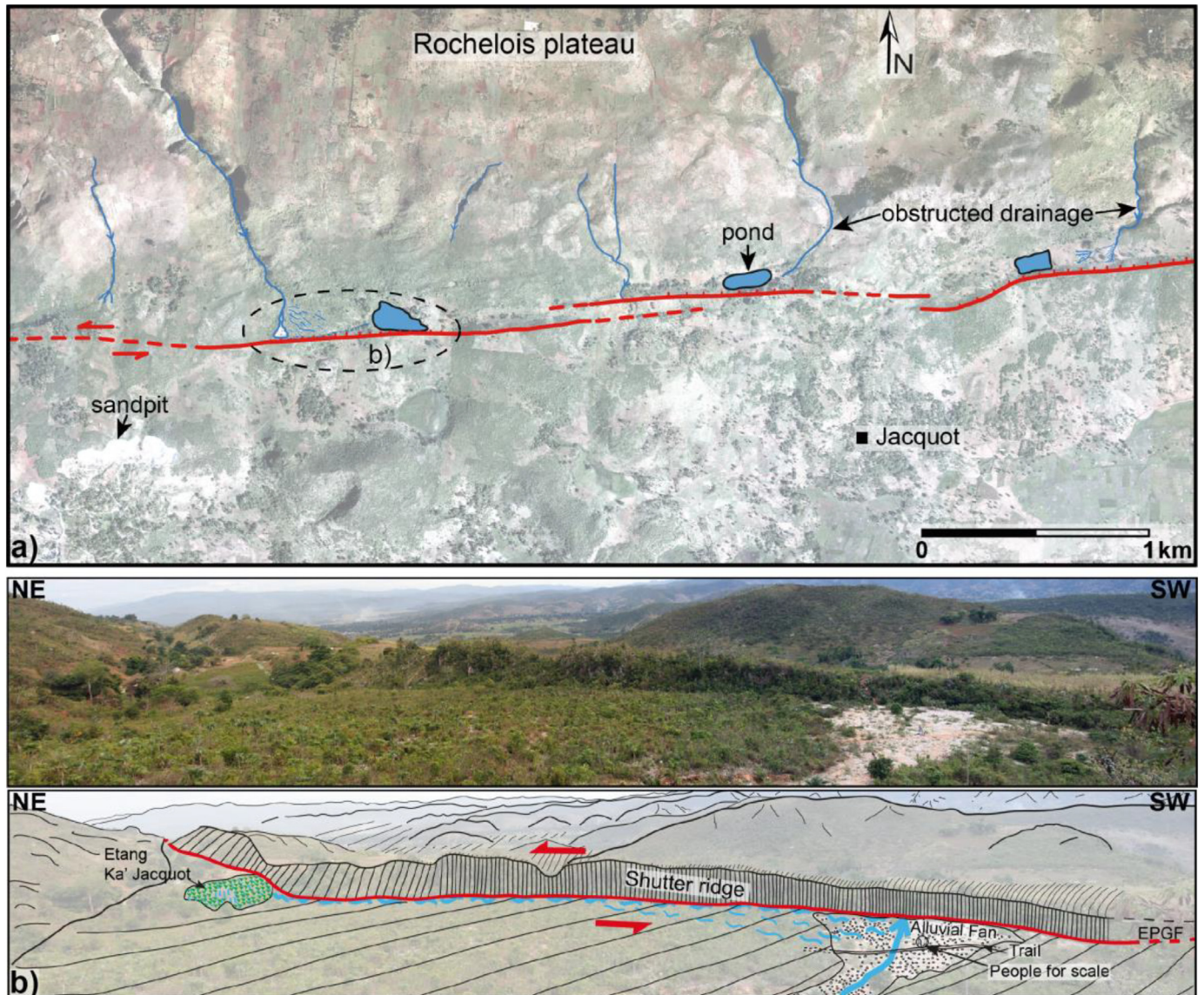
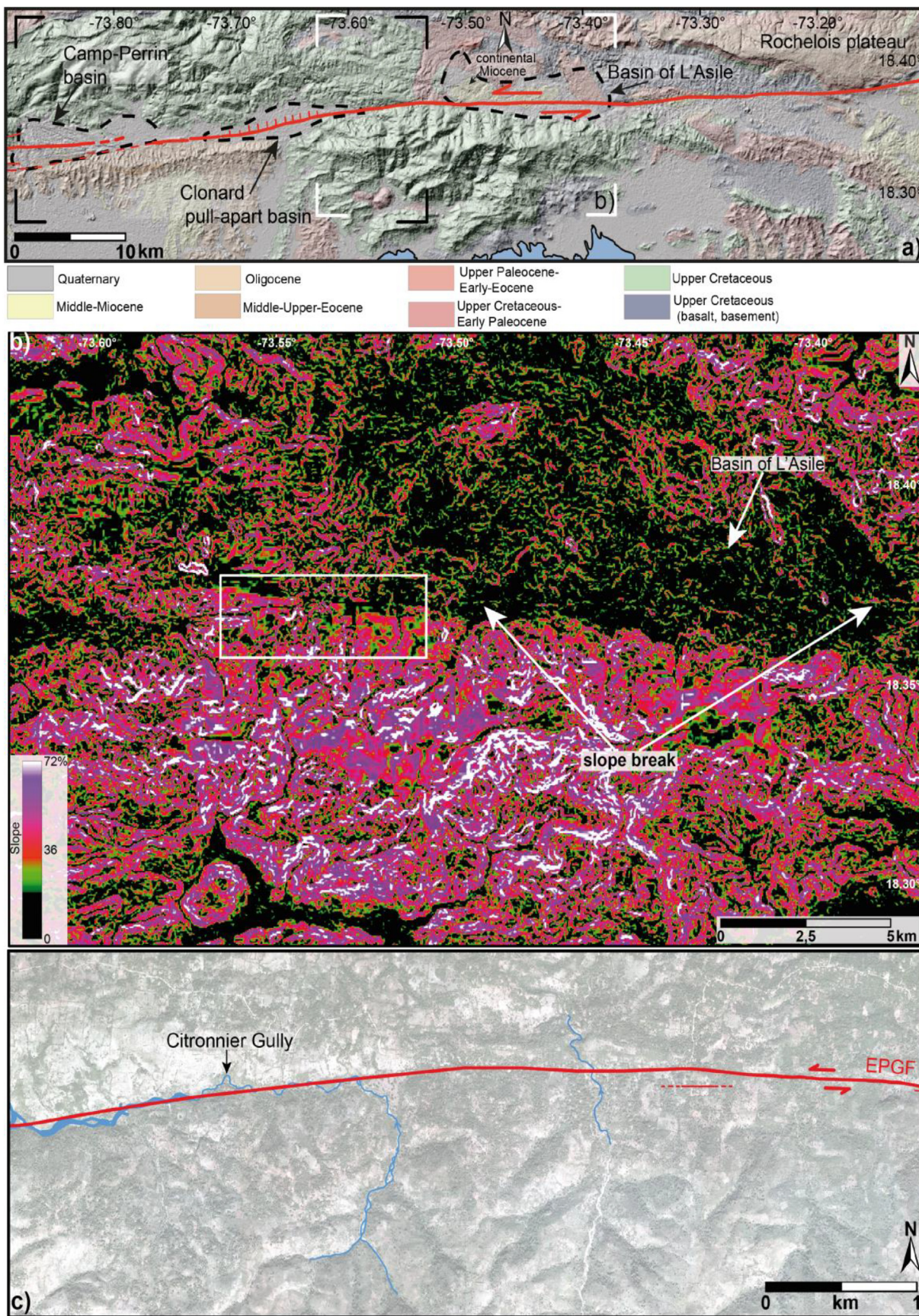


**Fig. 9.** a) Aerial photograph (pixel: 30 cm) of Jacquot area. The south-flowing drainages are deflected or obstructed by the fault. The streams pond in front of the fault scarp as shown by the basins. The dotted ellipse locates (b). b) Field photo mosaic and interpretation of Etang Ka' Jacquot (Ka' Jacquot pond) area. The drainage abuts against a ~10-m fault scarp that acts as a shutter ridge.

humus, clay and silt. The three first units step down to the south (Fig. 14b, c) whereas the overall morphology of the fault scarp at the surface shows a down-thrown to the north. This suggests that -only a secondary branch of the fault was exposed in our trench, the main fault being likely further south. The units 1, 2 and 3 are vertically offset by ~20 cm by that branch.

Above the offset units, we identified a dark greyish unit (unit number 4 in Fig. 14c), which is much thicker on the northern compartment of the fault. This unit was likely deposited after an earthquake to fill the accommodation space created by the vertical coseismic deformation (i.e, the depressed area on the downthrown side of the fault). This suggests the existence of a paleoseismic horizon between units 3 and 4. The unit 5 is uniformly thick (up to 1 m-thick), horizontal and

not deformed. It was deposited after the complete levelling of the coseismic scarp by the unit 4. Overall, the architecture of the fault growth sequence strongly supports the record of the last paleoearthquake at this place. The earthquake offset by the same quantity (20 cm) the three lower “pre-seismic” units. The unit 4 and 5 are post-seismic sedimentary units. The coseismic offset of 20 cm recorded by the lower units is on an individual secondary branch of the fault. The 2 m-high scarp in the landscape likely corresponds to the last coseismic vertical offset along the main branch of the fault. The unit 5 is much thicker (up to 1 m-thick) than the other units and was deposited by a recent spate of Cavaillon River, as confirmed by eyewitnesses. Though the sedimentation dynamics at this place is ideal for preserving the entire fault sequence during a complete seismic cycle, we could not unfortunately



(caption on next page)

**Fig. 10.** a) Geologic context of Clonard pull-apart, Camp-Perrin and L'Asile basins. Data: 1/250000 geological map [Moplaisir and Boisson, 1988] overlain on ASTER shaded DEM (pixel: 30 m). White and black boxes are locations of (b) and Fig. 11, respectively. b) Slope map of L'Asile basin area derived from ASTER DEM. In the basin, the slopes are ranging roughly from 0 to 36%. The colour palette shows more contrast for the slopes ranging from 20 to 36% in order to evidence the fault trace. The white box is the location of (c). c) Aerial photograph (pixel: 30 cm resized into 1 m) and interpretation of the western basin of L'Asile. The fault controls the course of Citronnier Gully.

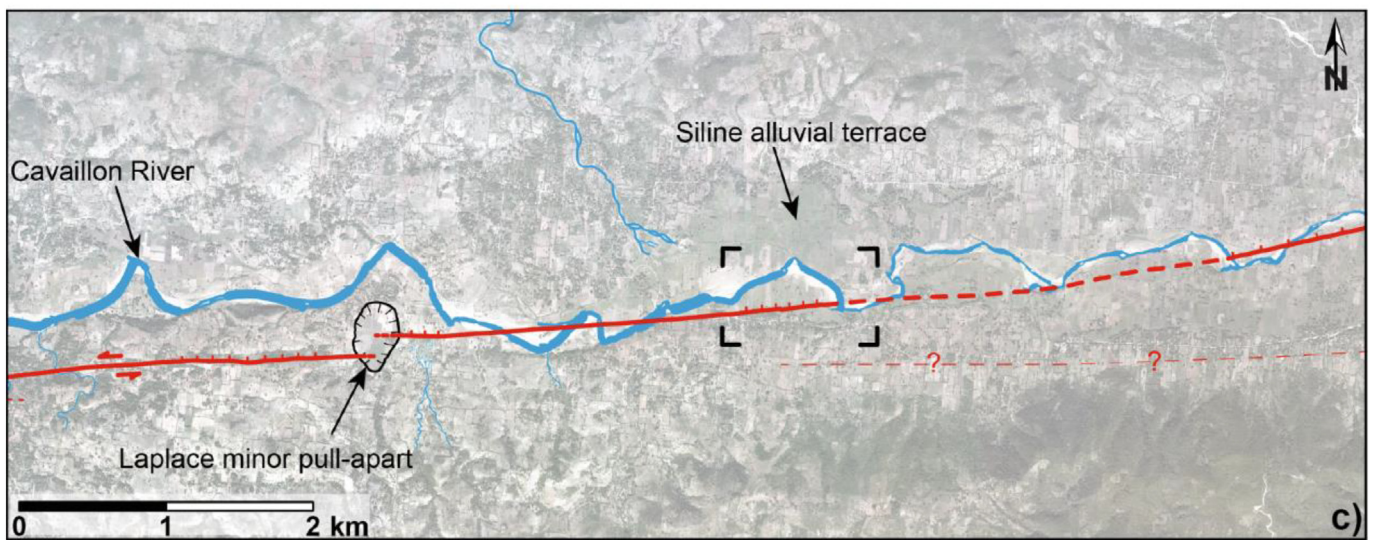
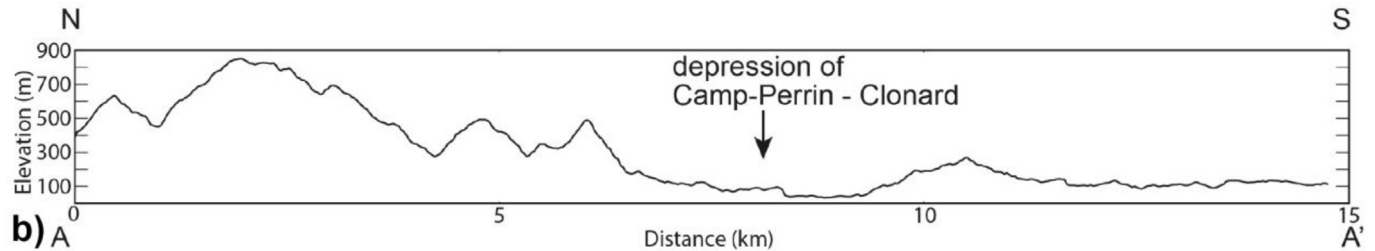
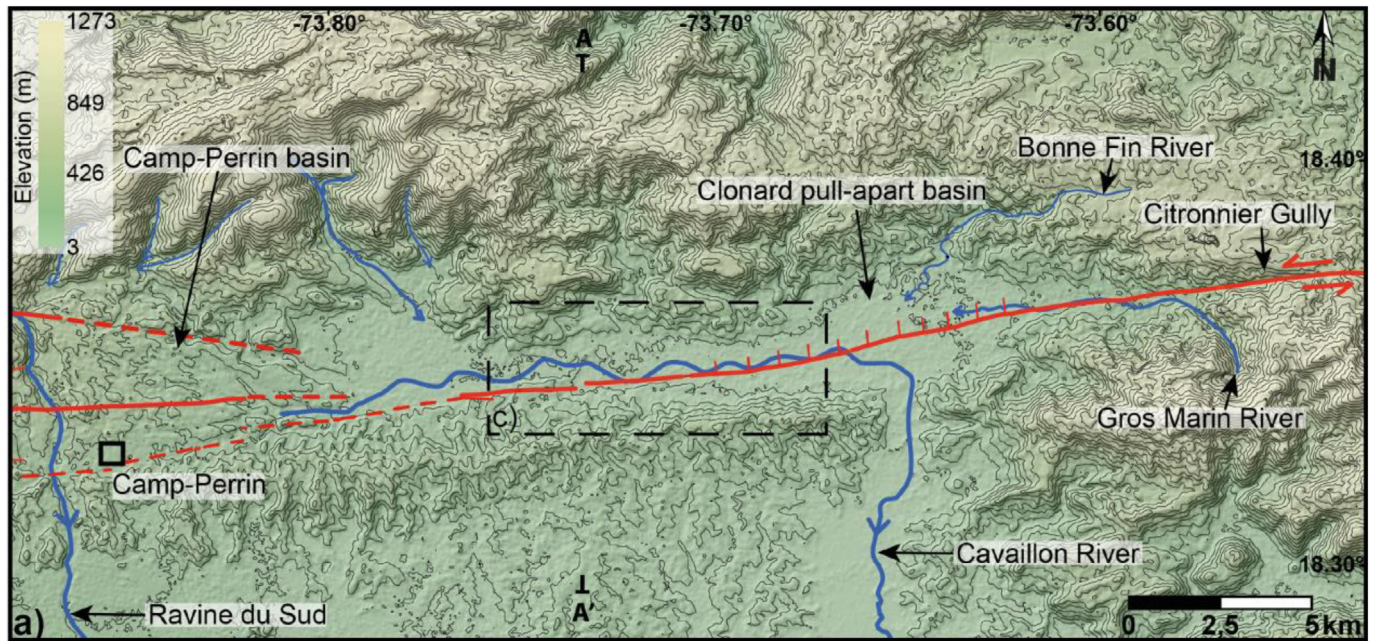


**Fig. 11.** a) Topographic map showing the Camp Perrin and Clonard pull-apart basins. In the two basins Cavaillon River is controlled by the EPGF. The dotted box is the location of (c). b) Topographic profile showing the depression zone of Camp Perrin - Clonard. Topographic data: ASTER (pixel 30 m). c) Map of the Enriquo-Plantain Garden Fault in the area of Cavaillon River, near the western edge of the Clonard pull-apart. Black box is the location of Fig. 13. Data: aerial photograph (pixel 30 cm).

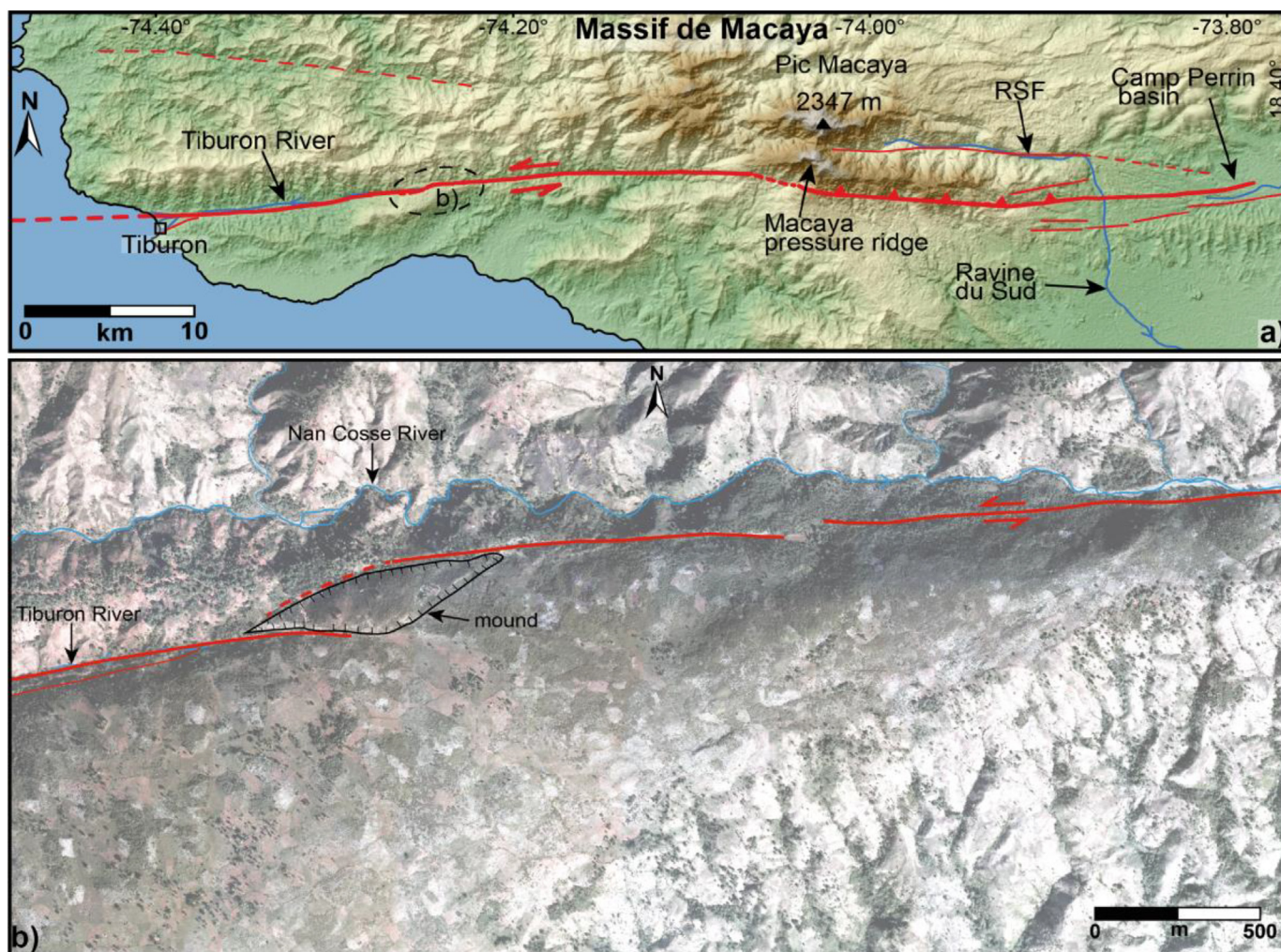


**Fig. 12.** a) Topographic map of the areas of Macaya and Tiburon River. The Pic Macaya (2347 m) is out the area of bordering faults. The Macaya pressure ridge is to the south of the peak (see text for discussion). RSF: Ravine du Sud Fault. The black dotted ellipse is the location of (b). b) Aerial photograph (pixel: 30 cm) of Nan Cosse River. Almost the whole southern wall of that river is encroached by the EPGF. The mound is discussed in Section 5.

find any organic material in our trench for direct radiocarbon dating. This is a classical difficulty in tropical environment where the organic matter oxidizes rapidly [e.g., Zech et al., 1997]. However, by chance we found a paleochannel exposure on one of the main riverbanks, at the immediate northern side of the fault (Fig. 15a). This riverbank is a natural cross-section that we cleaned in order to expose well the paleochannel. We found that the paleochannel was approximately at the same corresponding depth as the bottom of the trench (Fig. 15b). Assuming that the fault scarp observed on the terrace was formed by the last event, we can infer that the paleochannel used to flow on that

terrace toward the main Cavaillon River prior to that event. Since the paleochannel was rich in charcoal, we collected samples to have a maximum age for the paleoearthquake. The samples are HA\_12-01, HA\_12-02, and HA\_12-03.

Fig. 16 shows the calibrated radiocarbon age for the three samples. We consider that the samples were part of the same unit. In details, regarding the probability density, the most probable dates for HA\_12-01 are ranging from 1717 to 1784 CE. For HA\_12-02 and HA\_02-03, we have 1728–1810 CE and 1726–1814 CE, respectively (in green on Fig. 16). According to the coherence of the two latter date

**Table 1**  
Accurate location of the potential trench sites identified through our detailed mapping.

Sites	Longitude	Latitude	Description
Laplace	-73.714646	18.350145	Well-defined site characterized by a minor pull-apart in the huge Camp-Perrin – Clonard valley.
Siline	-73.692107	18.348457	Site of our exploratory trench. It is located in the Clonard pull-apart, on an alluvial terrace. See text for details.
Easter Clonard	-73.635782	18.360795	Well-defined site in the Clonard pull-apart basin [Mann et al., 1995; This study]
L'Asile 1	-73.503962	18.373775	Site located at the western edge of the basin of L'Asile. This site is chosen with uncertainties on the fault trace and/or sedimentary record.
L'Asile 2	-73.322251	18.372547	Site located at the eastern edge of the L'Asile basin. This site is chosen with uncertainties on the fault trace and/or sedimentary record.
Eastern Jacquot	-73.156105	18.379147	Well-defined site with stratigraphic evidence.
Fayette	-72.540099	18.471470	Site investigated by Gold et al. (2012)
Dumay 1	-72.190605	18.512608	Site investigated by Gold et al. (2012) and Saint Fleur et al. (2015, 2019)
Dumay 2	-72.174967	18.512568	Site investigated by Gold et al. (2012)

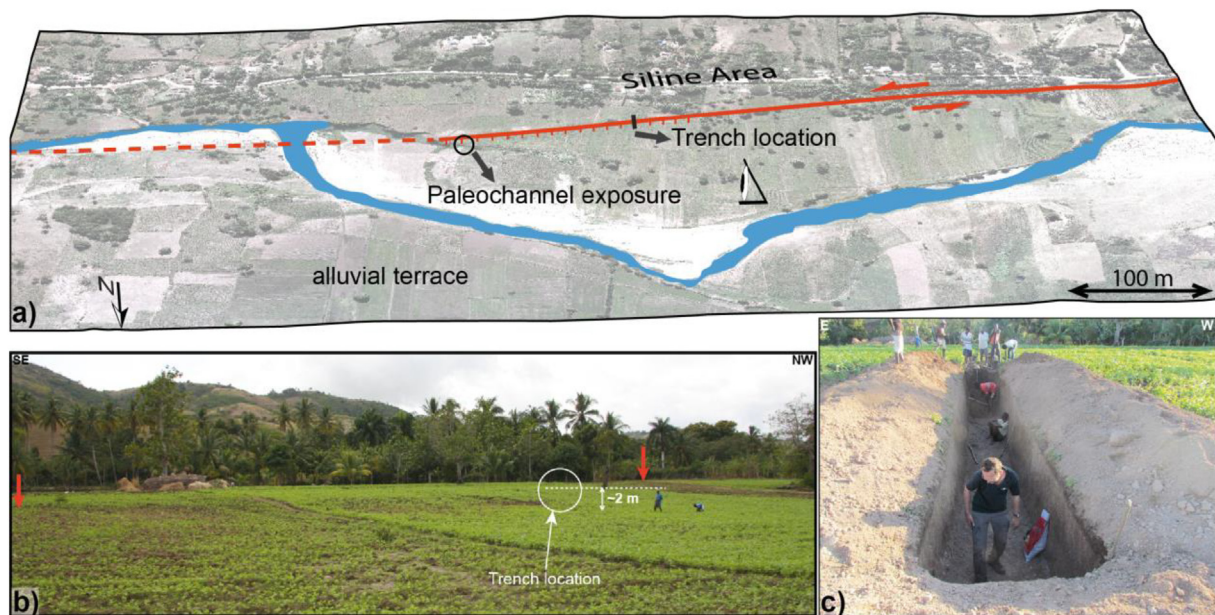


**Fig. 13.** The Siline area characterized by a terrace of Cavaillon River that is crosscut by the fault (see Fig. 11 for location). This site has been investigated for paleoseismological study. The eye looks at the approximate direction to which the field photograph in (b) was taken. Data: aerial photograph (pixel: 30 cm) overlain on ASTER DEM (pixel: 30 m). b) Field photograph of a ~2-m fault scarp in the Siline area. The fault is well expressed in spite of regular flooding and agricultural activities. Note the location of the trench. c) The exploratory trench manually excavated in Siline area. This trench is ~14-m long, 1.5-m wide and 1.5-m depth.

ranges, they are the most representative of the real age of the paleochannel. Thus, the date of deposition of the paleochannel is 1726–1814 or 1770 ± 44 CE.

## 5. Discussion

### 5.1. Paleoseismology

Considering that no event was attributed to the EPGF in the early 1800s [Bakun et al., 2012], the event found in our exploratory trench may be one of the eighteenth century's events (1701, 1751 or 1770).

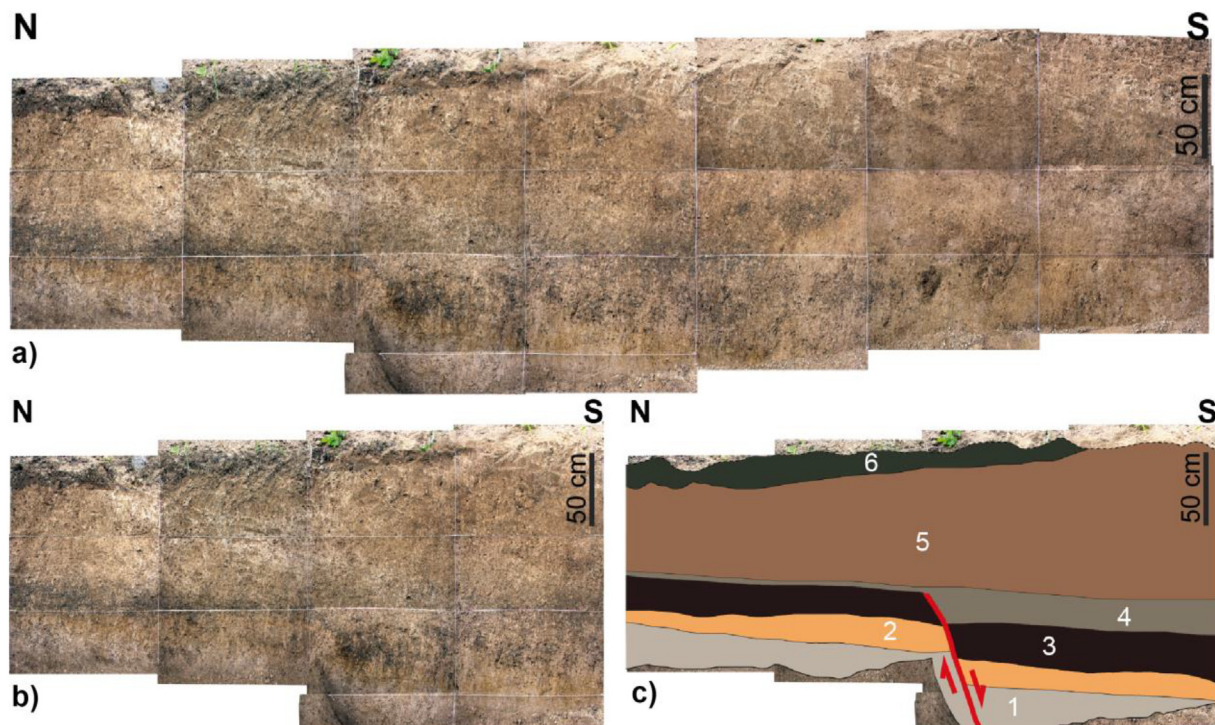


**Fig. 14.** a) Photo mosaic of the eastern wall of the trench. The rectangles are 1 × 0.5 m. b) Zoom on the left half of the eastern wall of the trench. c) Log of the sedimentary units exposed in the trench. 1 is roughly sandy whereas 2, 3, 4 and 5 are between silt and clay. Unit 6 being the arable soil. Units 1, 2 and 3 are offset by the fault during the last event in the area.

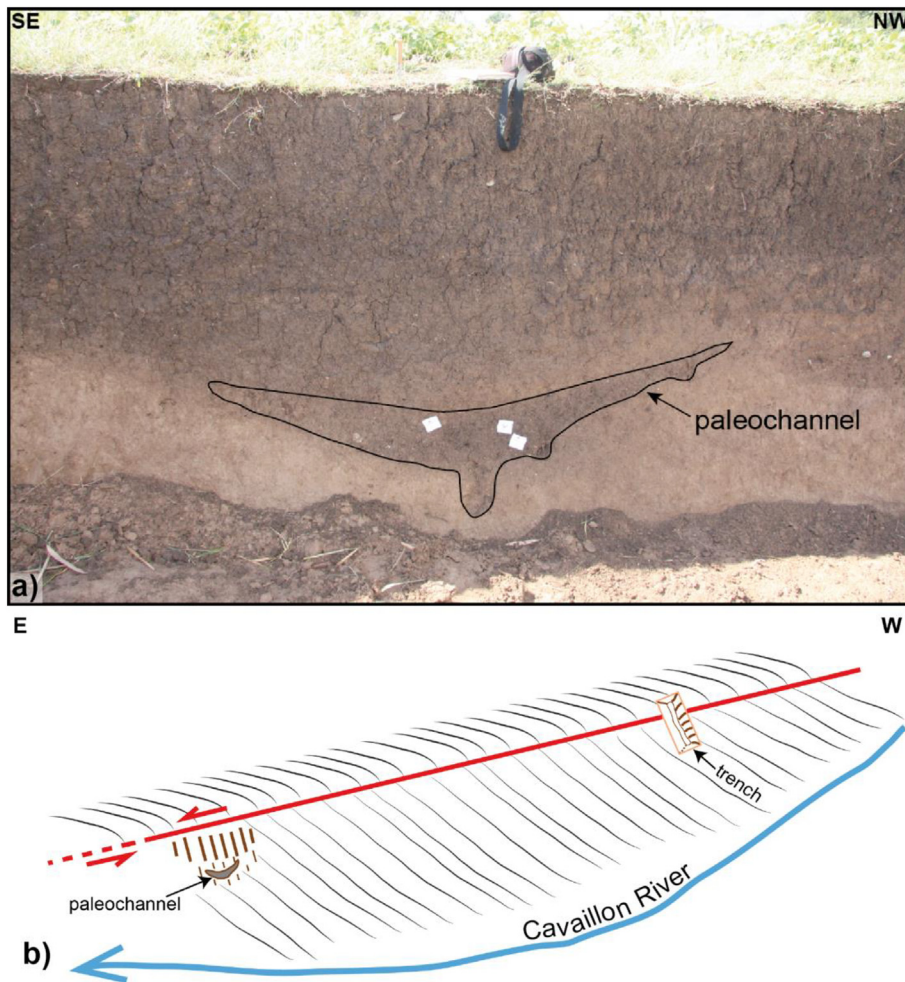


**Fig. 15.** a) Paleochannel exposure in the Siline alluvial terrace (see Fig. 13a for location). While no organic material was found in the exploratory trench, this paleochannel was rich in charcoal. Note the three samplings of the charcoal in the paleochannel. b) Sketch showing the position of the paleochannel with respect to both the fault trace and the trench. The paleochannel is at a similar depth than the bottom of the trench.

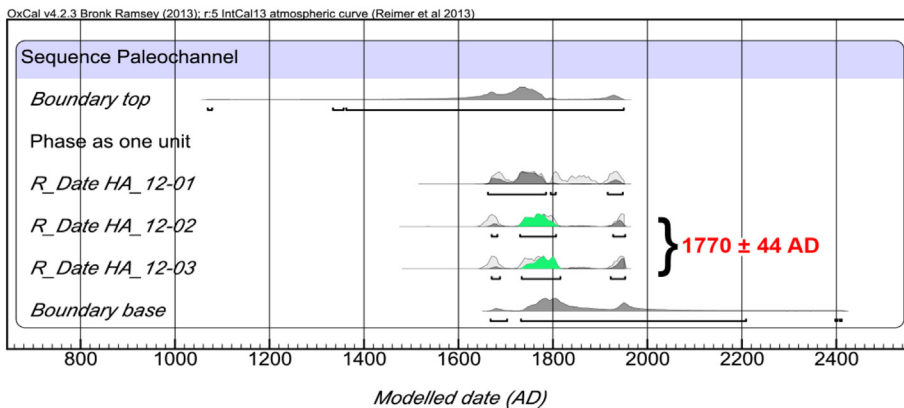


**Fig. 16.** The modelled dates (Ramsey, 2010, 2013; Reimer et al., 2013) of the radiocarbon ages of the three charcoal samples (HA 12-01, HA 12-02 and HA 12-03). The most probable date of deposition of the paleochannel is 1726–1814 or  $1770 \pm 44$  CE. Since the 1770 earthquake tends to be attributed to the segment through which the trench was excavated, the ground-ruptured event found in our exploratory trench may be the 1770 historical one. The dates are given with 95% of confidence interval.

The maximum intensities of the 1701 and the 1751 events were reported in Léogâne and Port-au-Prince. In addition, the 1701 event caused severe damage from the Cul-de-Sac plain to Petit-Goâve, the 1751 (21 November) event also caused severe damage in Port-au-Prince and in the Cul-de-Sac plain [Moreau de Saint Méry, 1803]. The latter reports rather suggest that the 1701 and 1751 events ruptured an eastern segment of the EPGF. However, for the 1770 event, the historical documents rather reported that the earthquake was felt in the entire island of Hispaniola and in Jamaica. In Haiti, this event severely

damaged the cities of Port-au-Prince, Léogâne, Petit-Goâve and particularly Les Cayes (Fig. 1), suggesting that it ruptured a western segment of the EPGF [Bakun et al., 2012; McCann, 2006]. Thus, the ground rupture found in our exploratory trench may be associated with the 1770 event. The vertical offset of ~20 cm found in our trench is quite large for a secondary fault branch and the 2 m-high scarp visible in the landscape likely corresponds to the vertical offset on the main fault. Such offsets are compatible with those observed for large strike slip earthquakes worldwide (e.g., Wells and Coppersmith, 1994; Klinger

et al., 2005) and support a large magnitude for the 1770 event which was one of the greatest earthquakes in Haiti. Such an event had the potential to cause severe damage in Port-au-Prince.

5.2. Lateral displacement along the EPGF

Our detailed fault mapping enabled us to evidence several sinistral offsets of several morphological and geological markers. They are of different scales, ranging from few meters to several tens of meters and even hundreds of meters and they attest for Quaternary activity of the fault. Although systematic dating of fault-offset markers would be require to establish precise model for seismic cycle along the different segments of the fault (i.e. to evidence Holocene characteristic coseismic slips for example), which is beyond the scope of this study, their analysis at different spatio-temporal scales is however still useful to get clues on the longer term activity and slip rate of the fault. As examples, by using morphometric parameters of the drainage network, Saint Fleur et al. (2019) have evidenced that the paleofan of Port-au-Prince and the Froide river are horizontally offset by ~8 km since Pleistocene times. The offset is larger westward as the Momance River is offset by ~15 km (Fig. 2), probably over the Plio-Pleistocene, considering an eastward propagation criterion. This implies a decrease of the slip rate from 4 to 6 mm/yr to 3 mm/yr eastward. In the following we described evidence of lateral offsets of much older geological markers by the EPGF, which helps to reconstruct the history of the faulting since the Pliocene.

5.2.1. Offset of the Massif de la Selle, the maximum offset of the EPGF along the southern peninsula of Haiti

The Massif de la Selle anticline is a ~N100°E, Lower Miocene anticline [Momplaisir and Boisson, 1988; Mann et al., 1995] that is

assumed to have been offset by the EPGF (Fig. 17) [Calais and Mercier de Lépinay, 1995; Calmus, 1983; Calmus and Vila, 1988; Heubeck and Mann, 1991a, 1991b; Mann et al., 1984; Van Den Berghe, 1983]. On the basis of our detailed fault map superimposed to the geological map and the topographic information, it is possible to describe in more detail the offset of the Massif de la Selle, as well as that of other anticlines further west, to get constraints on slip rates and the timing of faulting at the scale of the southern peninsula (Figs. 17 and 18). The morphology of the present-day northern edge of the anticline to the south of the Léogâne Delta Fan suggests that this anticline is sharply crosscut and offset by the fault.

A striking observation is that the Cretaceous tholeiitic complex (dark blue) of the core of the anticline is sharply disrupted by the fault and outcrops against the Quaternary unit of the Léogâne Delta Fan. The same geological units were mapped north of the fault. They form the core of another anticline ~40 km further west, which is disrupted and in sharp contact with cretaceous volcanic units to the north and Quaternary units to the south. This anticline composes the Fort-Royal hill.

The Massif de la Hotte is another anticline, having the same orientation than the Massif de la Selle. It is also sharply cut to the north by the EPGF.

North of Lake Miragoâne (Figs. 8 and 17) the Fort-Royal hill is likely the offset northern closure of the Massif de la Selle fold. It cannot be the offset counterpart of the Massif de la Hotte anticline because in the latter case, the offset is smaller (8 km) than that of the Momance River (15 km) which is located at the same place and which is likely younger. By considering that the fault extends eastwards to branch the contractional horsetail splays composed of the Dumay thrust and other reverse faults in the Cul-de-Sac – Enriquillo plain, we attempted a first

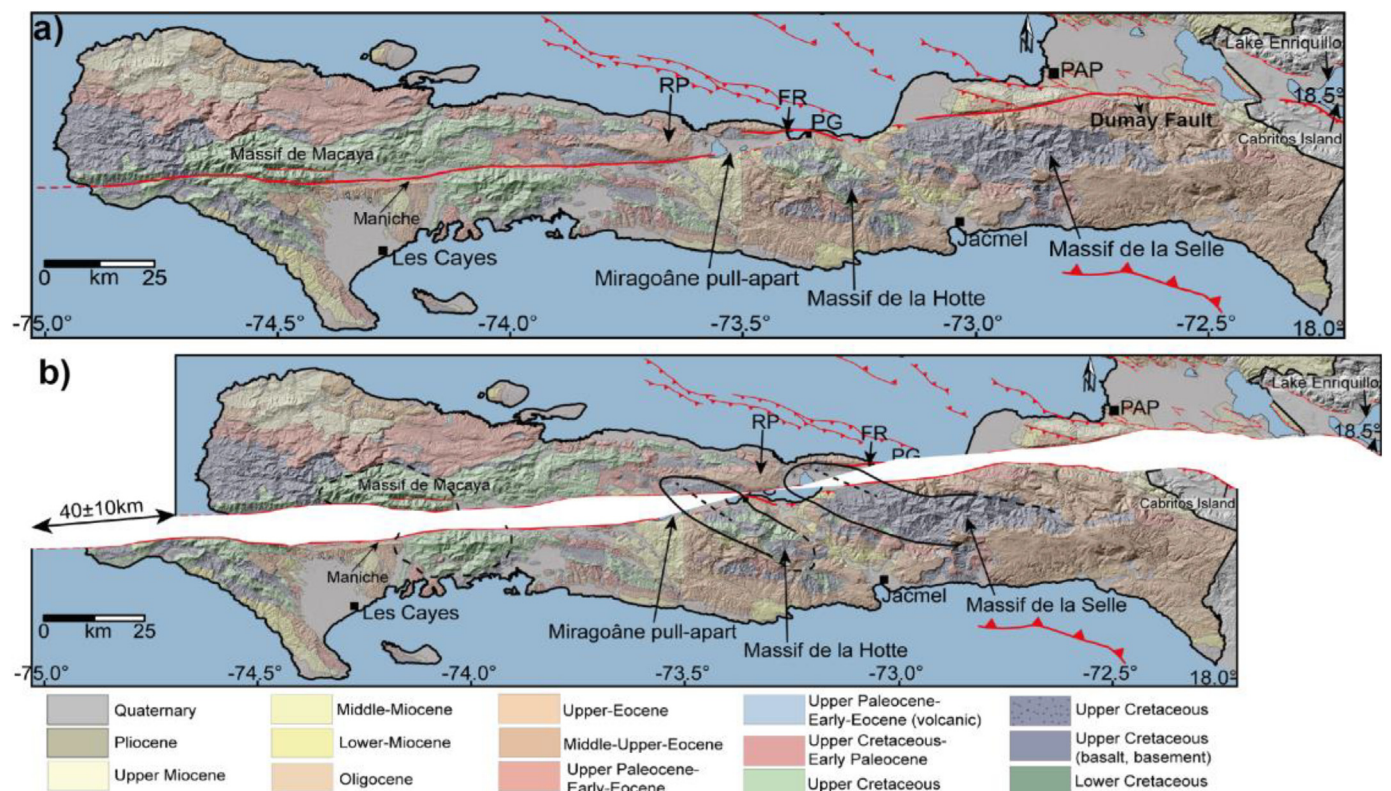
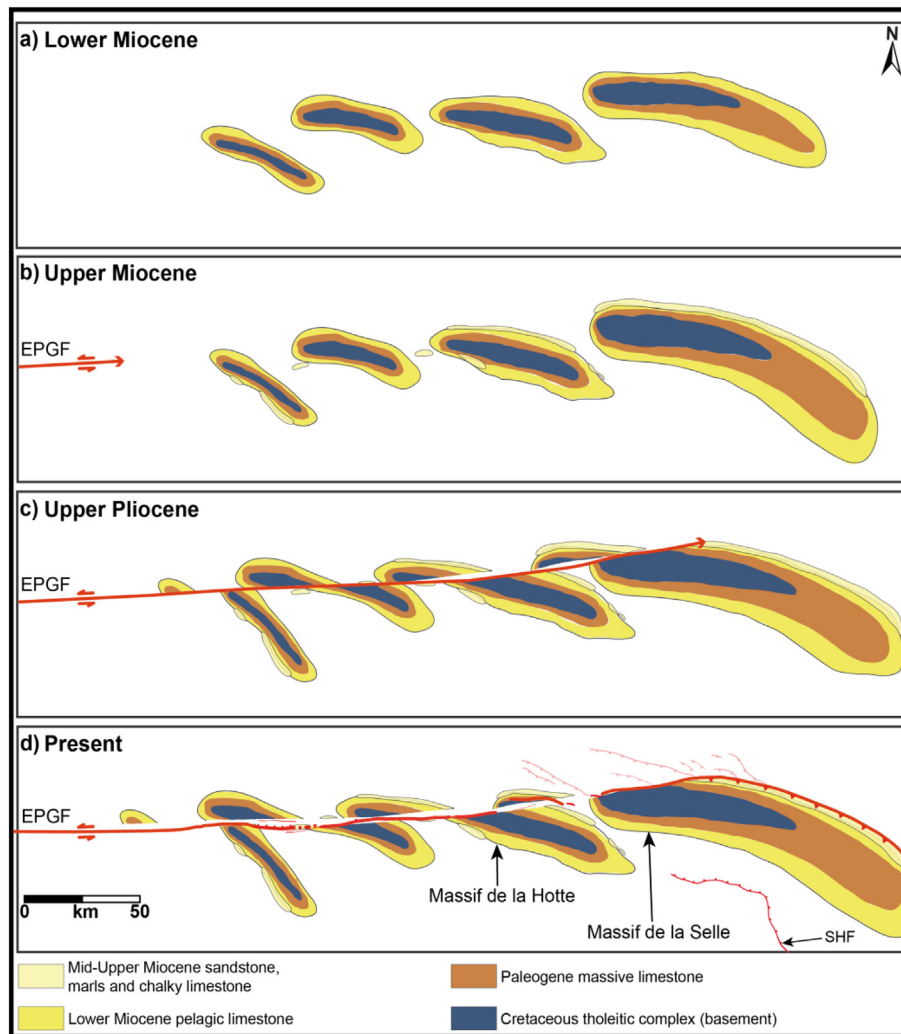


Fig. 17. a) Geomorphologic map of the southern peninsula showing several geologic units offset by the Enriquillo-Plantain Garden Fault (EPGF). PAP: Port-au-Prince; PG: Petit-Goâve; FR: Fort-Royal; RP: Rochelois Plateau. b) Tectonic reconstruction of maximum geological offset found in the southern peninsula of Haiti. The Massif de la Selle anticline (eastern fold) is obviously offset by the EPGF; its northern corresponding structure is likely the Fort-Royal hill. When we reconstruct the Massif de la Selle, the eastern massif de la Hotte (western fold) is reconstructed. The dotted black lines mimic approximate fold axes [Mann, 1983; Mann et al., 1995; Vila et al., 1985]. The 40 ± 10 km are obtained by passing the fault to the south and in the center, respectively, of the Miragoâne pull-apart. The latter estimate is also obtained by following the mapped reverse section of the fault to the east (Dumay Fault). The large uncertainty is due to the fold axes that are not well constrained.



**Fig. 18.** Sketch showing the eastward propagation of the Enriquillo-Plantain Garden Fault (EPGF) and its relationship with the inherited Lower Miocene folds in the southern peninsula based on observations reported in different studies [e.g., Calais and Mercier de Lépinay, 1995; Heubeck and Mann, 1991a, 1991b; Mann et al., 1991a; Mann et al., 1995; Pindell et al., 1988; Saint Fleur et al., 2015, 2019]. SHF: Southern Hispaniola Fault.

reconstruction of the Massif de la Selle anticline. We obtain offsets slightly different when the trace of the EPGF changes in the Miragoâne lake region, which is a 5 km large pull-apart. It is  $37 \pm 10$  km when the fault runs south of the pull-apart and it is  $40 \pm 10$  km when we consider that the fault cuts across the center of the pull-apart. We also tried a reconstruction by considering that the EPGF prolongates until the northern edge of the Cabritos Island (Lake Enriquillo, Dominican Republic), which morphology was previously assumed to be controlled by a section of the EPGF [Mann et al., 1995]. We obtained an offset of  $41 \pm 10$  km (Fig. S4).] Thus, we retained an average offset of about  $40 \pm 10$  km (Fig. 17b). With such a value, it is also possible to reconstruct the Massif de la Hotte anticline. The Cretaceous tholeiitic core of the southern part of the anticline strikingly corresponds to the same geological units which outcrop in the L'Asile basin. However, uncertainties are quite large because the fold axes are not well located. Nevertheless, our estimate is comparable to those found by Calmus (1984) and Van Den Berghe (1983) by using other markers in the field only. Regarding the river offset (Momance and Froide) to the east over the Pleistocene and the Plio-Pleistocene, respectively, the offset of the Massif de la Selle and the Massif de la Hotte to the west should have happened earlier, likely during the Early-Middle Pliocene. The  $40 \pm 10$  km would imply a slip rate of  $9 \pm 3$  mm/yr. The latter is higher than those to the east (4–6 and 3 mm/yr) inferred from the offsets of Momance and Froide rivers, respectively (Table 2).

The decrease of the geological offsets and related slip rates from west to east is consistent with the magnetic data of Pindell et al. (1988). Fig. 18 mimics the eastward propagation of the EPGF. The NW-SE folds forming the highlands of the southern peninsula are inferred to be of Lower Miocene age as their borders are made of Lower Miocene rocks (Fig. 18a). Mid-Upper Miocene rocks unconformably deposited on the folds. At the same time, the EPGF, having an eastward propagation, arrived in the area of the Jamaica passage, west of the southern peninsula of Haiti (Fig. 18b). The EPGF continued to propagate, entering the peninsula and beheading the Lower Miocene folds. Since the propagation was progressing, the amount of the western offsets increased while new offsets were setting up to the east (Fig. 18c). Fig. 18d shows the present-day situation where the Massif de la Hotte and Massif de la Selle are offset by  $40 \pm 10$  km. To the east of the Massif de la Selle, the fault zone mainly accommodates compressive deformation that is distributed on several thrust faults. This is a fold-propagation-thrust due to the suture between the southern peninsula and the island-arc, and to the present-day Hispaniola-Bahamas platform  $\sim 45^\circ$ -shortening direction in the area [Saint Fleur et al., 2015; Wang et al., 2018]. In addition to the regional shortening, such a pattern is consistent with the propagation direction [Perrin et al., 2016] of the EPGF and the fact that the main shear zone stops in the area [Saint Fleur et al., 2019].

**Table 2**  
Geologic left-lateral offsets and slip rates along the EPGF.

Markers	Approximate location along fault (lat/lon)	Offset amount (km)	Probable offset timing	Slip rate (mm/yr)	Source
Massif de la Hotte and Massif de la Selle anticlines	18.40°/ -72.93° and 18.45°/ -72.60°	40 ± 10	Early-Middle Pliocene	9 ± 3	This study
Momance river	18.47°/ -72.47°	~15	Plio-Pleistocene	4-6	This study
Froide river and Port-au-Prince paleofan	18.48°/ -72.37° and 18.50°/ -72.28°	~8	Pleistocene	~3	Saint Fleur et al. (2019)

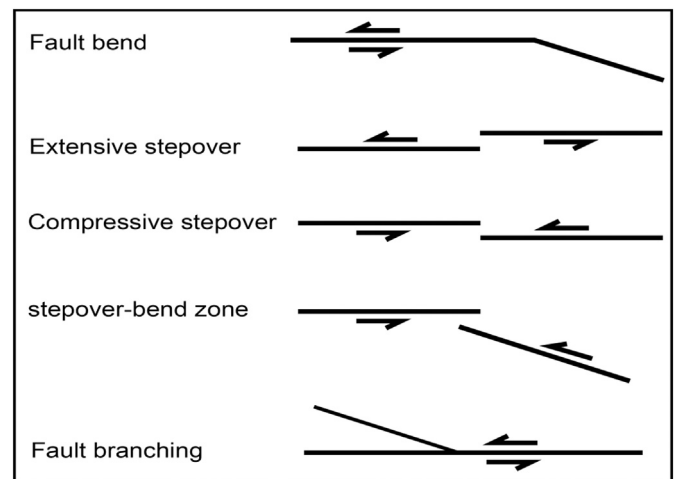


**Fig. 19.** Typical geometric complexities along a left-lateral strike-slip fault: fault bend (fault azimuth change), jog or relay zone or stepover that can be extensive or compressive, stepover-bend zone (a combination of the two previous cases), and fault branching.

### 5.3. First-order segmentation of the EPGF and seismic hazard

Fault segmentation represents a critical piece of information to constrain seismic cycle models and various scaling laws [Klinger, 2010; Schwartz and Coppersmith, 1984; Sieh, 1996; Weldon et al., 2004]. Here, as no surface rupture map is available, our segmentation is based on structural observations such as the superficial geology or the fault geometry [Klinger, 2010]. The segments are separated by geometric complexities or discontinuities [Knuepfer, 1989]. These geometric complexities are mainly fault azimuth change, jog or relay zone, jog-bend zone and fault branching (Fig. 19).

It has been observed that large earthquake ruptures are generally bounded by a fault azimuth change of > 30° [Barka and Kadinsky-Cade, 1988]. But bends do not often exceed a few degrees.

The jogs can be extensive or compressive, depending on the sense of the steps with respect to the sense of fault motion. The jogs may initiate, slow and stop rupture propagation [Barka and Kadinsky-Cade, 1988; Duan and Oglesby, 2006; Harris et al., 1991; King and Nabelek, 1985; Klinger et al., 2006; Klinger, 2010; Knuepfer, 1989; Sibson, 1986; Wesnousky, 1988, 2006]. Again, the size of a jog plays an important role. Analyzing 22 historical surface rupture maps, Wesnousky (2006) showed that earthquake ruptures cannot propagate through jogs that exceed ~5-km large.

Along the southern peninsula of Haiti, the strike-slip deformation is relatively obvious. However, to the east of Pétiion-Ville the trace of the EPGF disappears where diffuse compressional deformation is observed [Saint Fleur et al., 2015, 2019]. This may partly correspond to an off-fault tip splay network.

During our detailed mapping, we identified both small-scale geometric asperities (tens of meters) as well as large-scale ones (few kilometers). The large-scale features, except azimuth change, do not necessarily stop a dynamic rupture [Harris et al., 1991; King and Nabelek, 1985; Sibson, 1986; Wesnousky, 2006]. But, they can initiate, accelerate or slow down rupture propagation, as it appears to be the case during the 14 November 2001 Kokoxili earthquake in Tibet [Vallée et al., 2008]. We consider only the kilometeric-scale discontinuities as segment endpoints. In other words, we only take into account fault steps and bends that build kilometeric-scale features (e.g., Macaya, Clonard). These discontinuities are the most susceptible to affect the dynamics of earthquake rupture [Duan and Oglesby, 2006; Harris and Day, 1993, 1999; Oglesby, 2008; Wesnousky, 2006, 2008]. As they are persistent over several seismic cycles, the segment lengths they delimit can be used as key parameters to estimate probable earthquake size

[Albee and Smith, 1966; Bonilla et al., 1984; Slemmons, 1977; Wells and Coppersmith, 1994; Wesnousky et al., 1984].

From Pétion-Ville to Fayette (at the outlet of Momance River), the EPGF portrays a well-defined strike of  $\sim N80^\circ E$ . But, detailed mapping and field investigation along the Momance valley show several sub-faults of different geometries. Indeed, the eastern meander of Fig. 5b is crosscut by a  $\sim N75^\circ E$  south-facing fault scarp, supported by field observation (Fig. 5e). This description alone may indicate that the fault is either north- or south-dipping. A south-dip may imply that the fault could even be normal or has a normal component. But, neither available seismic data nor geomorphic observation allows confirming this. A north-dip would suggest a reverse component in the area. However, at only  $\sim 100$  m to the west, we observed a fault exposure that is  $\sim N100^\circ E$ -striking and dips  $60^\circ$  to the south. Since the latter faults are too different in strike and dip over relatively short distance, they cannot be representative of the overall geometry of the EPGF. Those minor faults may represent surface complexities of the main fault or secondary fractures, which are common in major strike-slip fault zones [Hobbs et al., 1976]. In addition, the minor faults mentioned above have very local actions. They portray scarps of a few meters and displace geomorphic features by a few meters to several tens of meters. Those minor faults do not appear to affect large-scale geomorphic features. At larger scale (Fig. 2), the main scarp is up to  $\sim 0.7$ -km high, albeit it may contain a part of apparent vertical, and portrays numerous related-uplift geomorphic features (Figs. 3 and 4) [Saint Fleur et al., 2015]. As the Massif de la Selle anticline is obliquely offset by the EPGF (Fig. 17), this topographic high may not be explained by an eventual dip toward the south of the EPGF as previously suggested [e.g., Prentice et al., 2010]. Fig. 21b shows a stack of 64 topographic profiles across the Massif de la Selle anticline. Its two flanks are well defined. Its crest is intensively eroded, consistent with the stretchiness and the sparseness of the profiles in the area. However, all the profiles are strikingly tight on the northern flank and particularly delineate a slope break corresponding to the EPGF. The topographic profiles systematically exhibit a regular slope to the south of- and a “bulge” north of the EPGF surface trace. This “bulge” unambiguously constitutes the main scarp of the EPGF that also offsets two long rivers: the Momance that is offset by  $\sim 15$  km, and Froide by  $\sim 8$  km. Such a geomorphic expression indicates that the main EPGF is constant in strike, probably steeply dips to the north, and constitutes a single segment from Pétion-Ville to Léogâne (Fayette in particular). We call this segment the Pétion-Ville – Léogâne segment (Fig. 20) [Saint Fleur et al., 2015].

From Dufort to Grand-Goâve, the EPGF trace is not seen in the morphology, but we only see evidence for reverse faulting (Fig. 7). Thus, in terms of geomorphology, it is difficult to see the continuation of the Pétion-Ville – Léogâne segment until Grand-Goâve. If we assumed that the EPGF continued, it would bend to the south by about  $10^\circ$ . This

configuration would imply a pull-apart extending from Dufort to Grand-Goâve, which would contradict the proposition of Cowgill et al. (2012) on the existence of a compressive stepover in the area. Their proposition was based on evidence for possible active folding (e.g., wind gap on Morne Diabie, Fig. 7a) along the southern margin of the Léogâne Delta Fan.

If the Dufort - Grand-Goâve section cannot be neither a compressive stepover nor a restraining bend, the observed evidence for reverse faulting should be independent from the geometry of the EPGF in the area. Thus, we propose that the reverse faults may be explained by a possible onland continuation of the  $\sim N120^\circ E$  Trois-Baies Fault (Fig. 7, inset). At the connection of the fault systems, the dip-slip deformation may be dominant, supporting the absence of surface strike-slip deformation in the area. Although it does not appear at the surface, the EPGF should be present in the  $\sim 17$ -km-long Dufort – Grand-Goâve section, as one needs this section to form the eastern bordering fault of the Tapion pressure ridge. In addition, as fault bends have been proven to be a robust criterion to distinguish discrete segments [Bilham and Williams, 1985; Klinger, 2010], the  $\sim 17^\circ$  of azimuth change of the EPGF along the Tapion pressure ridge must separate two distinct segments. The northern bordering fault of the Tapion pressure ridge is to the south of Fort-Royal hill. The latter fault, adding to its possible extension through the bay of Petit-Goâve, is about 15-km long. Thus, the Fort-Royal and Dufort – Grand-Goâve sections appear to have lengths for typical individual seismic segments [Klinger, 2010]. One can also consider the area extending from Dufort to western Lake Miragoâne as a huge geometric complexity: the  $\sim 45$ -km-long Léogâne – Miragoâne Complex Zone (LMCZ).

Then, from western Lake Miragoâne to western basin of L'Asile, the EPGF lies along a well-defined single trace (Figs. 8 and 10). The fault is  $\sim N85^\circ E$ -striking. However, the dip of the fault is difficult to constrain. For example, in the Fond-des-Nègres area, the fault exhibits a general north-facing scarp of  $\sim 10$ – $20$ -m high that affects the Paleogene limestone (Figs. 8 and 9). Since no geophysical data are available to constrain the fault structure at depth in this area, the north-facing scarp may be related to an either north- or south-dip. A dip to the north would indicate a normal (extensional) component in the area. A normal component appears to be in agreement with the ponds on Fig. 9. However, the hydrogeological context may be favorable as well to the formation of the ponds. A dip to the south would indicate a reverse (compressional) component. But, during our field investigations we did not see any tectonic feature that would be associated with a reverse component. Hence, in the absence of any geophysical data at depth, we assume that the fault is vertical in the area. In this case, the north-facing scarp is likely related to an apparent vertical or shutter ridge. The simple geometry, albeit in variable scarp heights, appears to continue westward through the basin of L'Asile. Thus, from western Lake

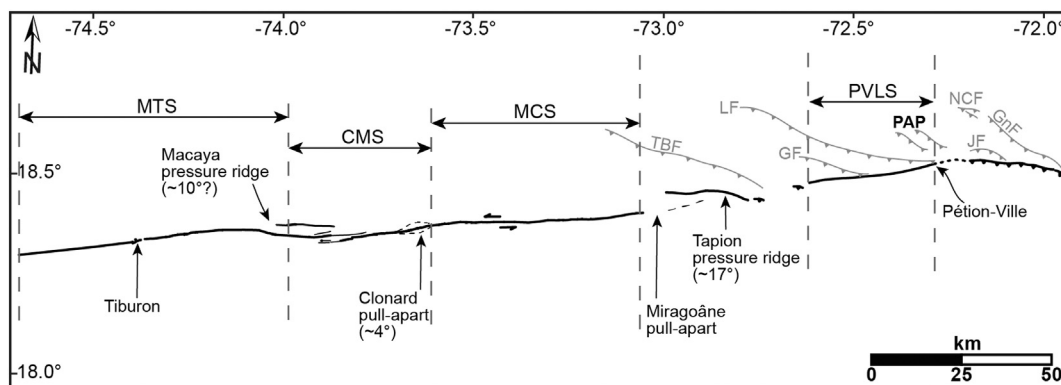
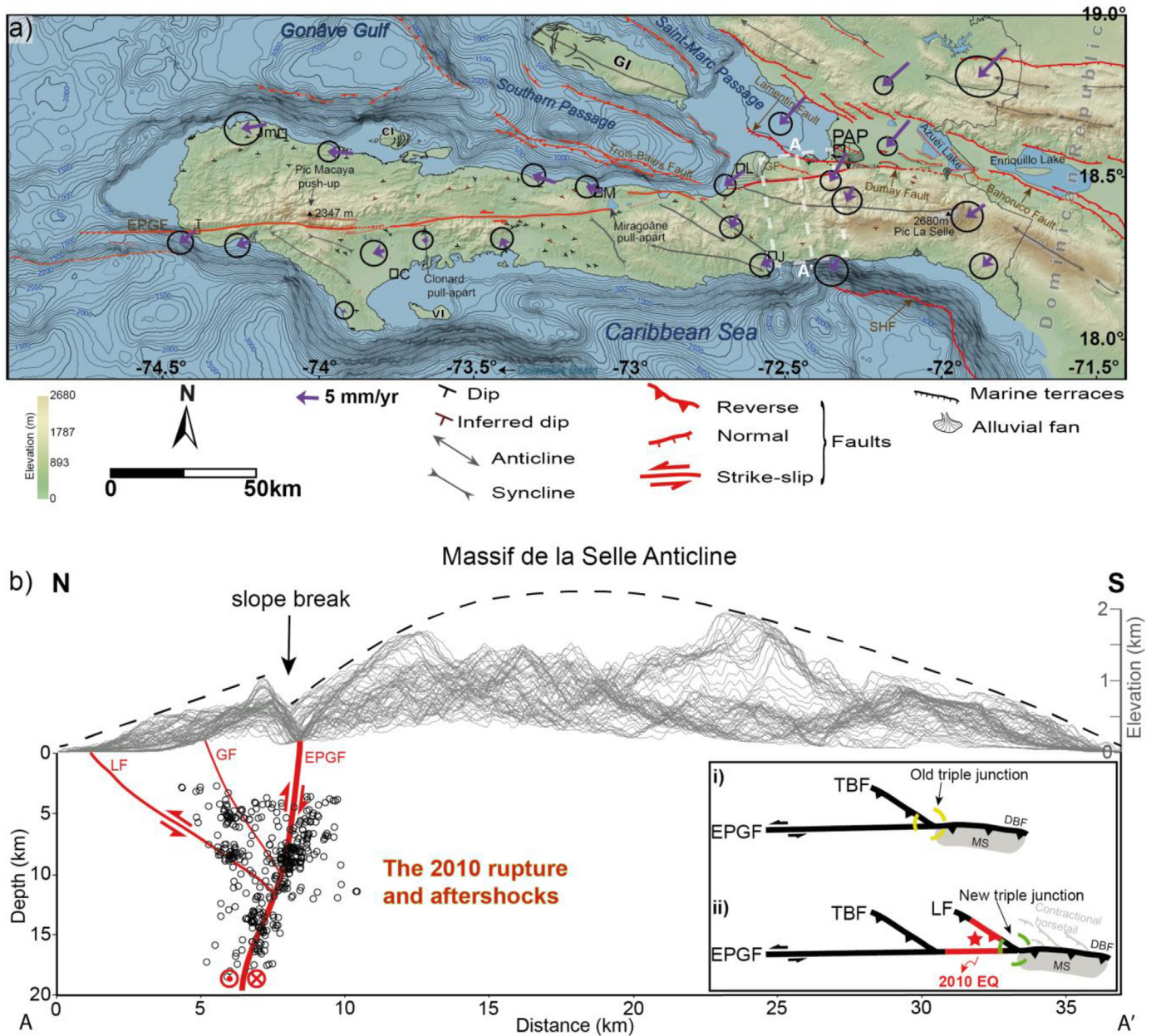


Fig. 20. Segmentation proposal of the Enriquillo-Plantain Garden Fault in the southern peninsula of Haiti. Four clear segments have been proposed in the peninsula. PVLS: Pétion-Ville – Léogâne segment; MCS: Miragoâne - Clonard segment; CMS: Clonard - Macaya segment; MTS: Macaya - Tiburon segment. TBF: Trois-Baies Fault; GF: Gressier Fault; LF: Lamentin Fault; JF: Jacquet Fault; NCF: Nan Cadastre Fault; GnF: Ganthier Fault; PAP: Port-au-Prince. See text for details.



**Fig. 21.** Seismotectonic synthesis of the southern peninsula of Haiti. a) Tectonic map with GPS vectors that depict pure strike-slip motion western Léogâne then transpression to the east. Error ellipses are 95% confidence. The GPS data are described in Calais et al. (2016). Topographic data: ASTER (30 m); Bathymetric data: SRTM30+; Isobaths are 100-m interval. b) Stack of 64 topographic profiles across the Massif de la Selle anticline in the area where the EPGF is conspicuous in the topography. The profiles' location is within the white box in a). The stack shows that the northern flank of the Massif de la Selle is crosscut by the EPGF. According to the stack, the main scarp of the EPGF is located to the north of its surface trace. The 2010 rupture and relocation of aftershock hypocenters (Douilly et al., 2013) are shown. Note the vertical scale for the depth is different from the one for the elevation. Inset is a sketch that mimics the evolution of a trench-trench-transform triple junction. i) Trois Baies Fault (TBF) was part of the triple junction; ii) As the EPGF propagates, the new triple junction is formed by the Lamentin Fault, the Dumay-Bahoruco Fault (DBF) and the EPGF. The 2010 rupture (in red) occurred near that triple junction. Red star: 2010 earthquake epicenter. EPGF: Enriquillo-Plantain Garden Fault; LF: Lamentin Fault; GF: Gressier Fault; SHF: Southern Hispaniola Fault; PAP: Port-au-Prince; L: Léogâne; J: Jacmel; M: Miragoâne; C: Cayes; T: Tiburon; Jm: Jérémie; Cl: Cayémites Island; Vi: Vache Island; Gi: Gonâve Island; MS: Massif de la Selle. (For interpretation of the references to colour in this figure legend, the reader is referred to the web version of this article.)

Miragoâne to western L'Asile (or eastern Clonard), the geometry of the EPGF is stable enough at the southern-peninsula scale to consider this stretch as a unique segment (Fig. 20). This is the Miragoâne-Clonard segment.

The EPGF bends along the middle of the Clonard pull-apart and continues along the basin of Camp-Perrin (Fig. 10). In this area, the fault does not exhibit a prominent scarp, except for the ~2-m-high scarp observed in the field [Mann et al., 1995; This study]. This morphology and geometry is relatively constant until eastern Macaya

pressure ridge. In addition, the ~4° of azimuth change of the fault in the Clonard pull-apart is sufficient to separate two distinct segments, as a fault bend of only 2° to 3° can significantly affect rupture propagation [Duan and Oglesby, 2006; King et al., 2005; Klinger et al., 2005; Klinger, 2010; Nielsen and Knopoff, 1998]. Thus, with ~4° of azimuth change, we can consider that we have a new segment extending from western Clonard to eastern Macaya: the Clonard-Macaya segment.

Then, the fault runs along southern Macaya pressure ridge (Fig. 12a). This pressure ridge is explained by an inferred ~10° bending

of the EPGF at the western edge of the ridge. The geometry of the ridge suggests that it may also be controlled by the Ravine du Sud Fault. To the west, the EPGF is well expressed along the terraces of Nan Cosse River before stepping down along Tiburon River. The relay zone of ~250-m wide between the two sub-faults should be a pull-apart while it is in fact a mound (Fig. 12b). We suggest that this mound be part of the overall topography both to the north and south of the fault. We then consider, at larger scale (Fig. 12a), that the two sub-faults are part of one segment: the Macaya-Tiburon segment.

In short, the detailed mapping of the EPGF has enabled us to distinguish at least four clear segments (Pétion-Ville – Léogâne; Miragoâne – Clonard; Clonard – Macaya; and Macaya – Tiburon) along the southern peninsula of Haiti (Fig. 20). We have also seen that the segments contain hundred-of-meter-scale asperities (e.g., Laplace minor pull-apart, Fig. 11) that would divide them into several sub-segments. These sub-segments may play a significant role in the initiation of seismic rupture but hardly stop it [Harris et al., 1991; King and Nabelek, 1985; Sibson, 1986; Wesnousky, 2006]. Using high-resolution satellite imagery, Klinger et al. (2011) mapped the 160-km long surface rupture of the 1931 Fuyun earthquake. From this mapping, they identified > 80 geometric complexities along the rupture trace. However, they proposed a first-order segmentation containing only 7 segments of 10 to 40 km long. Their segments were characterized by the greater geometric complexities, but mainly by their faulting style supported by their related long-term geomorphic features.

Similarly, we rather consider the southern-peninsula-scale segments separated by kilometer-scale, geometric complexities. From east to west, the Macaya – Tiburon segment starts western Macaya pressure ridge and continues several kilometers offshore of the town of Tiburon. Beside the Clonard – Macaya segment, which is 32 km long, the others are ~50-km long in average. However, the Clonard – Macaya segment is separated from the Miragoâne – Clonard one by a relatively small azimuth change (~4°), so a large earthquake from one of those segments may go through that geometric complexity and break both segments at the same time. For example, since Port-au-Prince was severely damaged and our paleoseismic investigation highlighted the 1770 event-related surface rupture along the Clonard-Macaya segment, the 1770 event might simultaneously break the two segments (Clonard – Macaya and Miragoâne – Clonard). Even if a rupture can go through the azimuth change, the segment change may be marked by change in faulting style probably normal, as in the case of the Mw 7.8, 2001 Kokoxili earthquake [King et al., 2005; Klinger et al., 2005; van der Woerd et al., 2002].

On the other hand, it appears very unlikely that a rupture starting along the Miragoâne – Clonard segment would reach the Pétion-Ville – Léogâne segment. This rupture should stop at the 5-km wide Miragoâne pull-apart, the western complexity of the LMCZ. Indeed, it has already been shown that stepovers wider than 3–5 km often arrest seismic ruptures [Harris et al., 1991; Wesnousky, 2006]. Alike, a rupture propagating westward along the Pétion-Ville – Léogâne segment would probably stop at the Tapion pressure ridge or the Miragoâne pull-apart. At the eastern edge of Tapion pressure ridge, the rupture may already encounter a first barrier, which is the branching of the Trois-Baies Fault. If possible, the rupture may preferentially continue along the Trois-Baies Fault. On the contrary, a rupture initiating along the Trois-Baies Fault may jump along the EPGF, as it was the case with the Lamentin Fault during the 2010 Haiti earthquake [Saint Fleur et al., 2015]. This has already been observed for several earthquakes where a secondary branch activated the main fault, and vice versa. This is related to the dynamic stress conditions at the branch in addition to the regional stress field and geometry [Klinger et al., 2017; Saint Fleur et al., 2015; Bhat et al., 2004; Kame et al., 2003; Sowers et al., 1994].

Overall, the geometry of the EPGF is simpler to the west where fault-branching is rare. One may consider that the fault is more mature western Miragoâne. To the east, compressional deformation and fault-branching begin to be salient with the Trois-Baies Fault. Then, the

pattern continues with the Lamentin Fault and the compression is more and more remarkable eastward. This pattern is strikingly highlighted by the GPS vectors that are slower and more parallel to the EPGF to the west and oblique to the east with increasing rates (Fig. 21a) [Calais et al., 2016]. As the eastern part is immature, it is more complex and active than the western part. More historical and instrumental earthquakes are recorded to the east [Bakun et al., 2012; Rodriguez et al., 2018]. The 2010 earthquake occurred in that complex, active zone. The active Lamentin thrust, as a branching fault, broke first and the rupture jumped to the EPGF (Fig. 21b) [Saint Fleur et al., 2015]. From a long-term kinematics point of view, that complex rupture occurred near a triple junction (Fig. 21b inset), as in the case of the Kaikoura, New Zealand 2016 earthquake [Shi et al., 2019]. Regarding the eastward propagation of the EPGF, the triple junction was first formed by the Troies Baies Fault, the Dumay Fault and the EPGF (trench-trench-transform geometry). Then, the Lamentin Fault replaces the Trois Baies Fault in the present-day triple junction. In this regard, like other western secondary thrusts, the Trois Baies Fault is as a remnant of the triple junction propagation but still active because its geometry is compatible with the regional stress field.

## 6. Conclusions

This work is a significant step for future studies of the Enriquillo-Plantain Garden Fault as it addresses several aspects. We have mapped the EPGF in detail using high-resolution imagery, geological data and field observations. This precise map can be used in the reconstruction perspective of Haiti.

Analyzing several criteria like fault geometry, sedimentary record and accessibility, several favorable sites for paleoseismic studies have been identified. An exploratory trench has been excavated in Siline area, in the basin of Clonard. That trench showed evidence for one paleoearthquake, which is likely the 1770 event. However, this preliminary result needs to be strengthened by more direct radiocarbon dating and excavation across the main fault.

The segmentation of the fault and seismic hazard implications have been discussed. We highlighted at least four clear segments by considering only kilometer-scale geometric complexities. More extensive paleoseismological studies may bring evidence for more segments as well as rupture scenarios along the Enriquillo-Plantain Garden Fault in Haiti.

Finally, the geological offsets of ~40, ~15 and ~8 km from west to east support the idea of an eastward propagation of the EPGF. In the easternmost part of the fault, east of Port-au-Prince, the fault zone rather portrays diffuse and compressional deformation, consistent with fault immaturity, the oblique convergence between Hispaniola and the Bahamas platform, and the indentation of the Beata Ridge in the area.

## CRedit authorship contribution statement

**Newdeskari Saint Fleur:** Conceptualization, Investigation, Methodology, Formal analysis, Writing - original draft. **Yann Klinger:** Investigation, Writing - review & editing, Validation. **Nathalie Feuillet:** Writing - review & editing.

## Declaration of competing interest

The authors declare that they have no known competing financial interests or personal relationships that could have appeared to influence the work reported in this paper.

## Acknowledgments

We thank INSU CT3 for funding and the Haitian Bureau of Mines and Energy, especially D. Anglade and O. Desliens for their assistance in the field. We are grateful to the ImageCat-RIT-Kucera International

team and to the World Bank GFDRR group for the LiDAR data. We also thank the National Center for Geospatial Information and B. E. Piard for providing the high-resolution aerial photographs. E. Calais kindly shared the GPS data with us and provided useful advice. We thank R. Lacassin, Y. Gaudemer, R. Gold, and C. Prentice for fruitful discussions. We are thankful to Paul Mann, and an anonymous reviewer for constructive comments to improve the quality of the paper.

## Appendix A. Supplementary data

Supplementary data to this article can be found online at <https://doi.org/10.1016/j.tecto.2020.228368>.

## References

- Albee, A.L., Smith, J.L., 1966. Earthquake characteristics and fault activity in southern California. In: *Engineering Geology in Southern California*, pp. 9–33.
- Ali, S.T., Freed, A.M., Calais, E., Manaker, D.M., McCann, W.R., 2008. Coulomb stress evolution in Northeastern Caribbean over the past 250 years due to coseismic, postseismic and interseismic deformation. *Geophys. J. Int.* 174 (3), 904–918.
- Bakun, W.H., Flores, C.H., ten Brink, U.S., 2012. Significant Earthquakes on the Enriquillo Fault System, Hispaniola, 1500–2010: Implications for Seismic Hazard. *Bull. Seismol. Soc. Am.* 102 (1), 18–30.
- Barka, Kadinsky-Cade, K., 1988. Strike-slip fault geometry in Turkey and its influence on earthquake activity. *Tectonics* 7 (3), 663–684.
- Bhat, H.S., Dmowska, R., Rice, J.R., Kame, N., 2004. Dynamic slip transfer from the Denali to Totschunda faults, Alaska: Testing theory for fault branching. *Bull. Seismol. Soc. Am.* 94 (6B), S202–S213.
- Bien-Aimé Moplaisir, R., 1986. Contribution à l'étude géologique de la partie orientale du Massif de la Hotte (Presqu'île du Sud d'Haïti): Synthèse structurale des marges de la presqu'île à partir de données sismiques. Thesis. Univ. Paris VI.
- Bilham, R., Williams, P., 1985. Sawtooth segmentation and deformation processes on the southern San Andreas fault, California. *Geophys. Res. Lett.* 12 (9), 557–560.
- Bonilla, M.G., Mark, R.K., Lienkaemper, J.J., 1984. Statistical relations among earthquake magnitude, surface rupture length, and surface fault displacement. *Bull. Seismol. Soc. Am.* 74 (6), 2379–2411.
- Brenner, M., Binford, M.W., 1988. A sedimentary record of human disturbance from Lake Miragoane, Haiti. *J. Paleolimnol.* 1 (2), 85–97.
- Calais, E., Mercier de Lépinay, B., 1995. Strike-slip tectonic processes in the northern Caribbean between Cuba and Hispaniola (Windward Passage). *Mar. Geophys. Res.* 17 (1), 63–95.
- Calais, É., Symithe, S., de Lépinay, B.M., Prépetit, C., 2016. Plate boundary segmentation in the northeastern Caribbean from geodetic measurements and Neogene geological observations. *Compt. Rendus Geosci.* 348 (1), 42–51.
- Calmus, 1983. Contribution à l'étude géologique du massif de Macaya (sud-ouest d'Haïti, Grandes Antilles): sa place dans l'évolution de l'orogène Nord-Caraïbe.
- Calmus, T., 1984. Décrochement Senestre Sud-Haïtien: analyses et conséquences paléogéographiques dans la région de Camp-Perrin (Massif de Macaya, presqu'île du Sud d'Haïti). *Ann. Soc. Géol. Nord. TC* 3, 309–316.
- Calmus, Vila, J.M., 1988. The Massif of Macaya (Haïti): the evolution of a Laramide structure in the left-handed-strike-slip boundary between North-America and Caribbean Plates. *Bol. Depto. Geol. Uni-Son* 5, 63–69.
- Cormier, M.H., Charles, N., Sloan, H., Wattrus, N., Sorlien, C., Boisson, D., ... Symithe, S., 2019. Multichannel Seismic Survey of Lake Azuei (Haiti) Documents a Complex System of Active Transpressional Structures Across the North American-Caribbean Plate Boundary. <https://doi.org/10.1002/essoar.10501580.1>.
- Cowgill, E., Bernardin, T.S., Oskin, M.E., Bowles, C., Yikilmaz, M.B., Kreylos, O., Elliott, A.J., Bishop, S., Gold, R.D., Morelan, A., 2012. Interactive terrain visualization enables virtual field work during rapid scientific response to the 2010 Haiti earthquake. *Geosphere* 8 (4), 787–804.
- Douilly, R., Haase, J.S., Ellsworth, W.L., Bouin, M.P., Calais, E., Symithe, S.J., ... Meremonte, M.E., 2013. Crustal structure and fault geometry of the 2010 Haiti earthquake from temporary seismometer deployments. *Bull. Seismol. Soc. Am.* 103 (4), 2305–2325.
- Duan, B., Oglesby, D.D., 2006. Heterogeneous fault stresses from previous earthquakes and the effect on dynamics of parallel strike-slip faults. *Journal of Geophysical Research: Solid Earth* (1978–2012) 111 (B5).
- Duplan, L., 1975. Photogeological survey of the southern area of the Republic of Haiti. In: *Rep. U. N. Min. Dev.* (edited).
- Gold, R.D., Prentice, C.S., Crone, A.J., Briggs, R.W., Narcisse, R., 2012. Evidence of Multiple, Prehistoric, Ground-Rupturing Earthquakes along the Enriquillo-Plantain Garden Fault System near Port-au-Prince, Haiti. (paper presented at AGU Fall Meeting Abstracts).
- Gorum, T., van Westen, C.J., Korup, O., van der Meijde, M., Fan, X., van der Meer, F.D., 2013. Complex rupture mechanism and topography control symmetry of mass-wasting pattern, 2010 Haiti earthquake. *Geomorphology* 184, 127–138.
- Harris, R.A., Day, S.M., 1993. Dynamics of fault interaction: parallel strike-slip faults. *Journal of Geophysical Research: Solid Earth* (1978–2012) 98 (B3), 4461–4472.
- Harris, R.A., Day, S.M., 1999. Dynamic 3D simulations of earthquakes on an echelon faults. *Geophys. Res. Lett.* 26 (14), 2089–2092.
- Harris, R.A., Archuleta, R.J., Day, S.M., 1991. Fault steps and the dynamic rupture process: 2-D numerical simulations of a spontaneously propagating shear fracture. *Geophys. Res. Lett.* 18 (5), 893–896.
- Heubeck, C., Mann, P., 1991a. Geologic evaluation of plate kinematic models for the North American-Caribbean plate boundary zone. *Tectonophysics* 191 (1), 1–26.
- Heubeck, C., Mann, P., 1991b. Structural geology and Cenozoic tectonic history of the southeastern termination of the Cordillera Central, Dominican Republic. *Geol. Soc. Am. Spec. Pap.* 262, 315–336.
- Higuera-Gundy, A., Brenner, M., Hodell, D.A., Curtis, J.H., Leyden, B.W., Binford, M.W., 1999. A 10,300 < sup > 14 < /sup > C yr record of climate and vegetation change from Haiti. *Quat. Res.* 52 (2), 159–170.
- Hobbs, B.E., Means, W.D., Williams, P.F., 1976. *An Outline of Structural Geology*. Wiley, New York.
- Kame, N., Rice, J.R., Dmowska, R., 2003. Effects of prestress state and rupture velocity on dynamic fault branching. *Journal of Geophysical Research: Solid Earth* (1978–2012) 108 (B5).
- King, G., Nabelek, J., 1985. Role of fault bends in the initiation and termination of earthquake rupture. *Science* 228 (4702), 984–987.
- King, G., Klinger, Y., Bowman, D., Tapponnier, P., 2005. Slip-partitioned surface breaks for the Mw 7.8 2001 Kokoxili earthquake, China. *Bull. Seismol. Soc. Am.* 95 (2), 731–738.
- Klinger, Y., 2010. Relation between continental strike-slip earthquake segmentation and thickness of the crust. *J. Geophys. Res.* 115 (B7).
- Klinger, Xu, X., Tapponnier, P., Van der Woerd, J., Lasserre, C., King, G., 2005. High-resolution satellite imagery mapping of the surface rupture and slip distribution of the Mw 7.8, 14 November 2001 Kokoxili Earthquake, Kunlun Fault, Northern Tibet, China. *Bull. Seismol. Soc. Am.* 95 (5), 1970–1987.
- Klinger, Michel, R., King, G., 2006. Evidence for an earthquake barrier model from Mw~7.8 Kokoxili (Tibet) earthquake slip-distribution. *Earth Planet. Sci. Lett.* 242 (3–4), 354–364.
- Klinger, Y., Etchebes, M., Tapponnier, P., Narteau, C., 2011. Characteristic slip for five great earthquakes along the Fuyun fault in China. *Nat. Geosci.* 4 (6), 389–392.
- Klinger, Y., Choi, J.H., Vallage, A., 2017. Fault branching and long-term earthquake rupture scenario for strike-slip earthquakes. *Fault zone dynamic processes: Evolution of fault properties during seismic rupture* 217–228.
- Kneupfer, P., 1989. Implications of the characteristics of end-points of historical surface fault ruptures for the nature of fault segmentation. In: *Fault Segmentation and Controls of Rupture Initiation and Termination*, pp. 89–315.
- Lacassin, R., Klinger, Y., Feuillet, N., 2013. Sismotectonique du tremblement de terre du 12 janvier 2010 en Haïti. *Outre-Terre* (1), 163–183.
- Leroy, S., Ellouz-Zimmermann, N., Corbeau, J., Rolandone, F., de Lépinay, B.M., Meyer, B., Burov, E., 2015. Segmentation and kinematics of the North America-Caribbean plate boundary offshore Hispaniola. *Terra Nova* 27 (6), 467–478.
- Manaker, D.M., Calais, E., Freed, A.M., Ali, S.T., Przybylski, P., Mattioli, G., ... De Chabalier, J.B., 2008. Interseismic plate coupling and strain partitioning in the northeastern Caribbean. *Geophys. J. Int.* 174 (3), 889–903.
- Mann, 1983. Cenozoic Tectonics of the Caribbean: Structural and Stratigraphic Studies in Jamaica and Hispaniola. PhD thesis, 688 pp. State Univ. of New York, Albany.
- Mann, Burke, K., Matumoto, T., 1984. Neotectonics of Hispaniola: plate motion, sedimentation, and seismicity at a restraining bend. *Earth Planet. Sci. Lett.* 70, 311–324.
- Mann, P., McLaughlin, P.P., Cooper, C., 1991a. Geology of the Azua and Enriquillo basins, Dominican Republic; 2, Structure and tectonics. *Geol. Soc. Am. Spec. Pap.* 262, 367–390.
- Mann, P., Draper, G., Lewis, J.F., 1991b. An Overview of the Geologic and Tectonic Development of Hispaniola. *Geological Society of America*.
- Mann, P., Taylor, F.W., Edwards, R.L., Ku, T.-L., 1995. Actively evolving microplate formation by oblique collision and sideways motion along strike-slip faults: an example from the northeastern Caribbean plate margin. *Tectonophysics* 246, 1–69.
- McCalpin, J., 1996. *Paleoseismology*. Academic Pr.
- McCann, W.R., 2006. Estimating the Threat of Tsunamiogenic Earthquakes and Earthquake Induced-Landslide Tsunami in the Caribbean. *World Scientific Publishing, Singapore*.
- Moplaisir, R., Boisson, D., 1988. Carte Géologique de la République d'Haïti, South-East sheet (Port-au-Prince). BME.
- Moreau de Saint Méry, M., 1803. Description topographique, physique, civile, politique et historique de Saint-Domingue. Philadelphia, 1797. La danse. Parme.
- Nielsen, S.B., Knopoff, L., 1998. The equivalent strength of geometrical barriers to earthquakes. *Journal of Geophysical Research: Solid Earth* (1978–2012) 103 (B5), 9953–9965.
- Oglesby, D., 2008. Rupture termination and jump on parallel offset faults. *Bull. Seismol. Soc. Am.* 98 (1), 440–447.
- Perrin, C., Manighetti, I., Gaudemer, Y., 2016. Off-fault tip splay networks: a genetic and generic property of faults indicative of their long-term propagation. *Compt. Rendus Geosci.* 348 (1), 52–60.
- Pindell, J.L., Cande, S.C., Pitman III, W.C., Rowley, D.B., Dewey, J.F., LaBrecque, J., Haxby, W., 1988. A plate-kinematic framework for models of Caribbean evolution. *Tectonophysics* 155 (1–4), 121–138.
- Posse, D., Keir, D., Harmon, N., Rychert, C., Rolandone, F., Leroy, S., Boisson, D., 2019. The tectonics and active faulting of Haiti from seismicity and tomography. *Tectonics* 38 (3), 1138–1155.
- Prentice, C., Mann, P., Crone, A.J., Gold, R.D., Hudnut, K.W., Briggs, R.W., Koehler, R.D., Jean, P., 2010. Seismic hazard of the Enriquillo-Plantain Garden fault in Haiti inferred from paleoseismology. *Nat. Geosci.* 3, 789–793.
- Ramsey, B., 2010. *OxCal 4.1 Manual*, Edited.
- Ramsey, B., 2013. *OxCal 4.2*, Edited.
- Reimer, P.J., Bard, E., Bayliss, A., Beck, J.W., Blackwell, P.G., Ramsey, C.B., Buck, C.E., Cheng, H., Edwards, R.L., Friedrich, M., 2013. *IntCal13 and Marine13 radiocarbon*

- age calibration curves 0–50,000 years cal BP. *Radiocarbon* 55 (4), 1869–1887.
- Rodriguez, J., Havskov, J., Sørensen, M.B., Santos, L.F., 2018. Seismotectonics of south-west Dominican Republic using recent data. *J. Seismol.* 22 (4), 883–896.
- Saint Fleur, N., Feuillet, N., Grandin, R., Jacques, E., Weil-Accardo, J., Klinger, Y., 2015. Seismotectonics of southern Haiti: a new faulting model for the 12 January 2010 M7.0 earthquake. *Geophys. Res. Lett.* 42 (23), 10–273.
- Saint Fleur, N., Feuillet, N., Klinger, Y., 2019. Active tectonics along the Cul-de-Sac-Enriquillo plain and seismic hazard for Port-au-Prince, Haiti. *Tectonophysics* 771, 228235.
- Schwartz, D.P., Coppersmith, K.J., 1984. Fault behavior and characteristic earthquakes: examples from the Wasatch and San Andreas fault zones. *Journal of Geophysical Research: Solid Earth* (1978–2012) 89 (B7), 5681–5698.
- Shi, X., Tapponnier, P., Wang, T., Wei, S., Wang, Y., Wang, X., Jiao, L., 2019. Triple junction kinematics accounts for the 2016 Mw 7.8 Kaikoura earthquake rupture complexity. *Proc. Natl. Acad. Sci.* 116 (52), 26367–26375.
- Sibson, R.H., 1986. Earthquakes and rock deformation in crustal fault zones. *Annu. Rev. Earth Planet. Sci.* 14, 149.
- Sieh, K.E., 1996. The repetition of large-earthquake ruptures. *Proc. Natl. Acad. Sci.* 93 (9), 3764–3771.
- Slemmons, D.B., 1977. State-of-the-Art for Assessing Earthquake Hazards in the United States. Report 6. Faults and Earthquake Magnitude Rep., DTIC Document.
- Sowers, J., Unruh, J., Lettis, W., Rubin, T., 1994. Relationship of the Kickapoo fault to the Johnson Valley and Homestead Valley faults, San Bernardino County, California. *Bull. Seismol. Soc. Am.* 84 (3), 528–536.
- Vallée, M., Landès, M., Shapiro, N.M., Klinger, Y., 2008. The 14 November 2001 Kokoxili (Tibet) earthquake: High-frequency seismic radiation originating from the transitions between sub-Rayleigh and supershear rupture velocity regimes. *Journal of Geophysical Research: Solid Earth* 113 (B7).
- Van Aardt, J.A., McKeown, D., Faulring, J., Raqueño, N., Casterline, M., Renschler, C., ... Antalovich Jr, J., 2011. Geospatial disaster response during the Haiti earthquake: a case study spanning airborne deployment, data collection, transfer, processing, and dissemination. *Photogramm. Eng. Remote. Sens.* 77 (9), 943–952.
- Van Den Berghe, B., 1983. Evolution sédimentaire et structurale depuis le Paléocène du secteur massif de la Selle (Haïti) «Baoruco»(République dominicaine)-«nord de la ride de Beata» dans l'orogène nord Caraïbe. Hispaniola-Grandes Antilles (PhD dissertation).
- Van den Bold, W.A., 1975. Neogene biostratigraphy (Ostracoda) of southern Hispaniola. *Bull. Am. Paleontol.* 66 (286), 599–639.
- Vila, Butterlin, J., Calmus, T., Mercier de Lepinay, B., Van den Berghe, B., 1985. Carte géologique d'Haïti au 1/1,000,000 avec notice explicative détaillée. Publication of CEGETCNRS, Bordeaux, France.
- Wang, J., Mann, P., Stewart, R.R., 2018. Late Holocene structural style and seismicity of highly transpressional faults in southern Haiti. *Tectonics* 37 (10), 3834–3852.
- Weldon, R., Scharer, K., Fumal, T., Biasi, G., 2004. Wrightwood and the earthquake cycle: what a long recurrence record tells us about how faults work. *GSA Today* 14 (9), 4–10.
- Wells, D.L., Coppersmith, K.J., 1994. New empirical relationships among magnitude, rupture length, rupture width, rupture area, and surface displacement. *Bull. Seismol. Soc. Am.* 84 (4), 974–1002.
- Wesnousky, S., 1988. Seismological and Structural Evolution of Strike-slip Faults.
- Wesnousky, S., 2006. Predicting the endpoints of earthquake ruptures. *Nature* 444 (7117), 358–360.
- Wesnousky, S., 2008. Displacement and Geometrical Characteristics of Earthquake Surface Ruptures: issues and Implications for Seismic-Hazard Analysis and the Process of Earthquake Rupture. *Bull. Seismol. Soc. Am.* 98 (4), 1609–1632.
- Wesnousky, S., Scholz, C., Shimazaki, K., Matsuda, T., 1984. Integration of geological and seismological data for the analysis of seismic hazard: a case study of Japan. *Bull. Seismol. Soc. Am.* 74 (2), 687–708.
- Wessels, R.J., Ellouz-Zimmermann, N., Bellahsen, N., Hamon, Y., Rosenberg, C., Deschamps, R., Leroy, S., 2019. Polyphase tectonic history of the Southern Peninsula, Haiti: from folding-and-thrusting to transpressive strike-slip. *Tectonophysics* 751, 125–149.
- van der Woerd, J., Mériaux, A.-S., Klinger, Y., Ryerson, F., Gaudemer, Y., Tapponnier, P., 2002. The 14 November 2001, Mw = 7.8 Kokoxili earthquake in northern Tibet (Qinghai Province, China). *Seismol. Res. Lett.* 73 (2), 125–135.
- Zech, W., Senesi, N., Guggenberger, G., Kaiser, K., Lehmann, J., Miano, T.M., Miltner, A., Schroth, G., 1997. Factors controlling humification and mineralization of soil organic matter in the tropics. *Geoderma* 79 (1), 117–161.